ARTICLE

Bi-allelic Mutations in *TTC29* Cause Male Subfertility with Asthenoteratospermia in Humans and Mice

Chunyu Liu,[1,2,3,12] Xiaojin He,[4,5,6,12] Wangjie Liu,[1,2,3,12] Shenmin Yang,[7,8,12] Lingbo Wang,[1,9,12] Weiyu Li,[1,2,3] Huan Wu,[4,5,6] Shuyan Tang,[1,2] Xiaoqing Ni,[4,5,6] Jiaxiong Wang,[8] Yang Gao,[4,5,6] Shixiong Tian,[1,2,3] Lin Zhang,[9] Jiangshan Cong,[1,2] Zhihua Zhang,[10] Qing Tan,[4,5,6] Jingjing Zhang,[4,5,6] Hong Li,[8] Yading Zhong,[11] Mingrong Lv,[4,5,6] Jinsong Li,[9] Li Jin,[1] Yunxia Cao,[4,5,6,*] and Feng Zhang[1,2,3,*]

As a type of severe asthenoteratospermia, multiple morphological abnormalities of the flagella (MMAF) are characterized by the presence of immotile spermatozoa with severe flagellar malformations. MMAF is a genetically heterogeneous disorder, and the known MMAF-associated genes can only account for approximately 60% of human MMAF cases. Here we conducted whole-exome sequencing and identified bi-allelic truncating mutations of the *TTC29* (*tetratricopeptide repeat domain 29*) gene in three (3.8%) unrelated cases from a cohort of 80 MMAF-affected Han Chinese men. *TTC29* is preferentially expressed in the testis, and TTC29 protein contains the tetratricopeptide repeat domains that play an important role in cilia- and flagella-associated functions. All of the men harboring *TTC29* mutations presented a typical MMAF phenotype and dramatic disorganization in axonemal and/or other peri-axonemal structures. Immunofluorescence assays of spermatozoa from men harboring *TTC29* mutations showed deficiency of TTC29 and remarkably reduced staining of intraflagellar-transport-complex-B-associated proteins (TTC30A and IFT52). We also generated a *Ttc29*-mutated mouse model through the use of CRISPR-Cas9 technology. Remarkably, *Ttc29*-mutated male mice also presented reduced sperm motility, abnormal flagellar ultrastructure, and male subfertility. Furthermore, intracytoplasmic sperm injections performed for *Ttc29*-mutated mice and men harboring *TTC29* mutations consistently acquired satisfactory outcomes. Collectively, our experimental observations in humans and mice suggest that bi-allelic mutations in *TTC29,* as an important genetic pathogeny, can induce MMAF-related asthenoteratospermia. Our study also provided effective guidance for clinical diagnosis and assisted reproduction treatments.

Introduction

Male infertility has been reported as a complex multifactorial pathological condition with highly heterogeneous phenotypic presentations ranging from the total absence of spermatozoa in the testis to obvious alterations of sperm quality.[1–3] Suboptimal semen qualities, including poorly motile sperm and abnormal sperm morphology, have become important factors leading to the inability to have offspring in 30%–50% of sub-fertile couples.[3,4]

Multiple morphological abnormalities of the flagella (MMAF) is one of the most severe sperm malformations. MMAF is characterized as asthenoteratospermia involving absent, short, bent, coiled, and/or irregular-caliber flagella without any other symptoms of primary ciliary dyskinesia (PCD).[5] MMAF is considered to be a disorder of genetic origin, and several genes have been reported to be responsible for sperm flagellar defects; these genes include *AK7* (MIM: 615364), *AKAP4* (MIM: 300185), *ARMC2* (MIM: 618424), *CFAP43* (MIM: 617558), *CFAP44* (MIM: 617559), *CFAP65* (MIM: 614270), *CFAP69* (MIM: 617949), *DNAH1* (MIM: 603332), *FSIP2* (MIM: 618153), *QRICH2* (MIM: 618304), *SPEF2* (MIM: 610172), *TTC21A* (MIM: 611430), and *WDR66* (also known as *CFAP251*, MIM: 618146).[6–19] However, previous findings only account for approximately 60% of human MMAF cases. These findings highlight the genetic heterogeneity of MMAF and the potential involvement of new genetic factors in asthenoteratospermia.

Cilia and flagella are microtubule-based organelles whose assembly requires a motile process, known as intraflagellar transport (IFT). IFT, first discovered in the green alga *Chlamydomonas reinhardtii*, was shown to rely on a bi-directional transport system directed by IFT protein complexes and motors.[20] IFT protein complexes have been distinguished into complexes A and B, and they contain approximately 20 IFT proteins in *Chlamydomonas*.[21] Previous studies have revealed that mutations in IFT protein

[1]Obstetrics and Gynecology Hospital, NHC Key Laboratory of Reproduction Regulation (Shanghai Institute of Planned Parenthood Research), State Key Laboratory of Genetic Engineering at School of Life Sciences, Fudan University, Shanghai 200011, China; [2]Shanghai Key Laboratory of Female Reproductive Endocrine Related Diseases, Shanghai 200011, China; [3]State Key Laboratory of Reproductive Medicine, Center for Global Health, School of Public Health, Nanjing Medical University, Nanjing 211166, China; [4]Reproductive Medicine Center, Department of Obstetrics and Gynecology, The First Affiliated Hospital of Anhui Medical University, Hefei 230022, China; [5]Anhui Province Key Laboratory of Reproductive Health and Genetics, Anhui Medical University, Hefei 230022, China; [6]NHC Key Laboratory of Study on Abnormal Gametes and Reproductive Tract, Anhui Medical University, Hefei 230022, China; [7]State Key Laboratory of Reproductive Medicine, The Affiliated Suzhou Hospital of Nanjing Medical University, Suzhou 215002, China; [8]Suzhou Municipal Hospital, Suzhou 215002, China; [9]State Key Laboratory of Cell Biology, Shanghai Key Laboratory of Molecular Andrology, CAS Center for Excellence in Molecular Cell Science, Shanghai Institute of Biochemistry and Cell Biology, Chinese Academy of Sciences, University of Chinese Academy of Sciences, Shanghai 200031, China; [10]Department of Epidemiology and Biostatistics, School of Public Health, Anhui Medical University, Hefei 230022, China; [11]Department of Radiology, The First Affiliated Hospital of Anhui Medical University, Hefei 230022, China
[12]These authors contributed equally to this work
*Correspondence: caoyunxia6@126.com (Y.C.), zhangfeng@fudan.edu.cn (F.Z.)
https://doi.org/10.1016/j.ajhg.2019.10.010.

complexes cause several ciliopathies and male infertility.[22–24] For example, IFT140 (a component of IFT complex A) is a key regulator for male fertility, and *Ift140*-mutated mice were infertile and affected by significantly reduced sperm counts and multiple morphological abnormalities.[22] Furthermore, IFT74, a component of IFT complex B, is also essential for spermiogenesis in mice.[24] Therefore, these animal studies support the association of IFT protein complexes with male fertility and suggest that more IFT transport genes could be involved in spermiogenesis or related ciliopathies.

In this study, we conducted genetic analyses in a large cohort of 80 MMAF-affected Chinese men through the use of whole-exome sequencing (WES). Interestingly, bi-allelic truncating mutations of *TTC29* (*tetratricopeptide repeat domain 29*) were identified in two unrelated consanguineous families and in one simplex individual. Furthermore, our generated *Ttc29*-mutated male mice also showed reduced sperm motility, abnormal flagellar ultrastructure, and damaged fertility. Despite poor upshots of *in vitro* fertilization (IVF) performed for *Ttc29*-mutated male mice, the intracytoplasmic sperm injection (ICSI) treatment showed that both *Ttc29*-mutated mice and men harboring *TTC29* mutations acquired satisfactory outcomes. These findings strongly suggest that bi-allelic mutations of *TTC29* can induce asthenoteratospermia and male subfertility in humans and mice.

Material and Methods

Study Participants

The cohort of 80 MMAF-affected Chinese men was enrolled from the First Affiliated Hospital of Anhui Medical University and the Affiliated Suzhou Hospital of Nanjing Medical University in China. All individuals presented with a typical MMAF phenotype characterized by severe asthenoteratospermia due to a combination of sperm flagellar defects as follows: absent, short, bent, coiled, and/or irregular-caliber flagella. Moreover, PCD-associated symptoms (such as sinusitis, bronchitis, pneumonia, and otitis media)[25] were reviewed very carefully and excluded from the MMAF cohort. Clinical investigation revealed that development of male external genitalia, bilateral testicular sizes, hormone levels, and secondary sexual characteristics were normal in all of the MMAF-affected men in this study. Peripheral whole blood samples were collected for genetic analyses. The chromosomal karyotypes are also normal (46; XY), and no large-scale deletions were found in the Y chromosome. This study was approved by the institutional review boards at Fudan University, the First Affiliated Hospital of Anhui Medical University, and the Affiliated Suzhou Hospital of Nanjing Medical University. Signed informed consent was obtained from all of the subjects participating in the study.

Whole-Exome Sequencing and Bioinformatic Analysis

Genomic DNA was isolated from peripheral blood samples from human subjects through the use of the DNeasy Blood and Tissue Kit (QIAGEN). 1 μg of genomic DNA was utilized to enrich the human exome through the use of the SureSelect XT Human All Exon Kit (Agilent). Next-generation sequencing was conducted with the Illumina HiSeq X-TEN platform at Cloud Health Genomics. Reads were mapped to the human genome reference assembly (GRCh37/hg19) by using Burrows Wheeler Aligner (BWA) software to put the original mapping result into BAM format.[26] Picard software was employed to remove PCR duplicates and evaluate the quality of variants. Then ANNOVAR software was used for functional annotation with information from OMIM, Gene Ontology, KEGG Pathway, SIFT, PolyPhen-2, MutationTaster, 1000 Genomes Project, ExAC, and gnomAD.[27–33] Finally, the variants with read depths less than 4 × were filtered out according to the Genome Analysis Toolkit.[34]

According to previous pedigree analyses, MMAF has been assumed to follow an autosomal recessive inheritance.[35,36] Therefore, we mainly focused on bi-allelic rare variants identified through WES. Considering the fact that MMAF leads to male infertility, the genetic variants with allele frequencies ≥ 0.01 in the human population genome datasets (e.g., the ExAC Browser and 1000 Genomes Project) were filtered out. Nonsense, frameshift, and essential splice-site variants were preferred. Missense variants predicted to be deleterious simultaneously by the bioinformatic tools of SIFT, PolyPhen-2, and/or MutationTaster were also included for further evaluation.

Semen Characteristics Analysis

Semen analysis was conducted in the source laboratories during routine biological examination of the individuals according to the World Health Organization (WHO) guidelines. Semen samples from the men harboring *TTC29* mutations (A002 IV-1, A038 IV-1, and S003 II-1) were collected through masturbation after 2–7 days of sexual abstinence and evaluated after liquefaction for 30 min at 37°C. Analyses of semen volume, sperm concentration, and motility were carried out and replicated in the source hospitals during routine examination. The morphology of the sperm cells was assessed with hematoxylin and eosin (H&E) staining and scanning electron microscopy (SEM) assay. For each subject, at least 200 spermatozoa were examined to evaluate the percentages of morphologically abnormal spermatozoa.

Semen samples from mice were collected from the cauda epididymides obtained through dissection of adult male mice and diluted in 1 mL solution of capacitation for 15 min at 37°C. Semen characteristics were further analyzed using a computer-assisted analysis system. At least three 8-week-old male C57BL/6 mice were analyzed for each group.

Electron Microscopy Evaluation

For SEM assay, the sperm specimens were deposited on poly-L-lysine-coated coverslips and immersed in 2.5% glutaraldehyde, rinsed in 0.1 mol/L phosphate buffer for 30 min, and post-fixed in osmic acid. After being rinsed thoroughly in the same buffer for 30 min, the specimens were progressively dehydrated with an ethanol and isoamyl acetate gradient and dried through the use of a CO_2 critical-point dryer (Eiko HCP-2, Hitachi). Afterward, the specimens were mounted on aluminum stubs, sputter coated through the use of an ionic sprayer meter (Eiko E-1020, Hitachi), and analyzed via SEM (Stereoscan 260) under an accelerating voltage of 20 kV.

For transmission electron microscopy (TEM), the prepared spermatozoa were washed and immersed in 2.5% phosphate buffered glutaraldehyde, washed with 0.1 mol/L phosphate buffer (PB, pH7.2) three times, and post fixed with 1% osmium tetroxide in

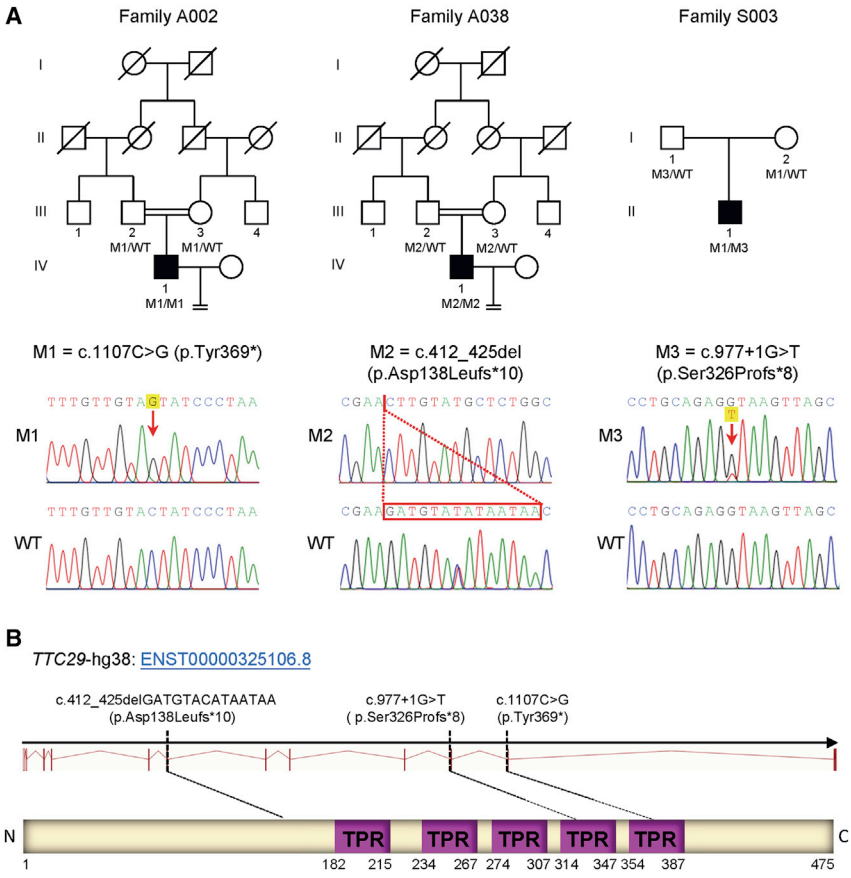

Figure 1. Identification of Bi-allelic Mutations in *TTC29*

(A) Pedigrees of three families carrying *TTC29* truncating mutations. All three affected individuals have bi-allelic mutations with a recessive inheritance mode. The probands from both consanguineous families A002 and A038 have homozygous truncating mutations in *TTC29*. The proband from family S003 carries compound heterozygous variants of *TTC29* derived from his parental, heterozygous carriers. Sanger sequencing results are shown below the pedigrees. The position of each variant is indicated by a red arrow or box.

(B) Schematic representation of the functional domains of TTC29 and locations of *TTC29* mutations identified in this study. The purple boxes indicate tetratricopeptide repeat domains as described by the Uniprot server. *TTC29* mutations are annotated in accordance to recommendations of the Human Genome Variation Society. Abbreviations: M1, mutation 1; M2, mutation 2; M3, mutation 3; WT, wild type.

0.1 mol/L PB for 1–1.5 h at 4°C. Dehydration was performed using graded ethanol (50%, 70%, 90%, and 100%) and 100% acetone followed by infiltration with 1:1 acetone and SPI-Chem resin overnight at 37°C. After infiltration and embedding in Epon 812, the specimens were sliced with ultra-microtome and stained with uranyl acetate and lead citrate, and then they were observed and photographed via TEM (TECNAI-10, Philips) with an accelerating voltage of 80 kV. For quantification of axonemal anomalies by TEM, at least 100 flagella with cross sections and several longitudinal sections were counted.

Real-Time Quantitative PCR and Reverse Transcription PCR

Total RNA of sperm was extracted using the RNeasy Mini Kit (QIAGEN) and converted into cDNAs using SuperScript III Reverse Transcriptase (Invitrogen) and oligo (dT) primers (TaKaRa). The obtained cDNAs were individually diluted 5-fold to be used as templates for the subsequent real-time fluorescence quantitative PCR with AceQ qPCR SYBR Green Master Mix (Vazyme). *GAPDH*/*Gapdh* was used as an internal control. The expression of mRNA was quantified according to the $2^{-\Delta\Delta Ct}$ method.

Immunoblot Analysis

The proteins of mouse sperm cells and testis tissues were extracted using Minute™ Total Protein Extraction Kit for Animal Cultured Cells and Tissues (Invent), then denatured at 95°C for 10 min. The denatured proteins were separated on 10% SDS-polyacrylamide gels and transferred to a polyvinylidene difluoride (PVDF) membrane (Millipore) for the immunoblot analysis. After a 1 h blocking step in 5% milk diluted with TBST (TBS-0.1% Tween-20), the membranes were incubated overnight at 4°C using the anti-TTC29 (PA5-70409, Invitrogen, 1:1000) directed toward the N-terminal region (14 amino acid immunogen in ARQKLPCSSRKIPRSQLIKE KDDIDHYLEVNFKEEVAYRNSYKKN) of the TTC29 protein and HRP-conjugated beta actin (HRP-60008, Proteintech, 1:2000) diluted in blocking buffer. Then the membrane was washed in TBST and incubated with HRP-conjugated secondary antibody (Abmart, M21002) at a 1:2500 dilution in blocking solution for 1 h at room temperature. After washing three times in TBST, blots were revealed using the Chemistar™ High-sig ECL Western Blotting Substrate (Tanon) with the Tanon 5200.

Immunofluorescence Analysis

Sperm cells were washed in phosphate buffer saline (PBS) and fixed in 4% paraformaldehyde for 30 min at room temperature and coated on slides which were pre-coated with 0.1% poly L-lysine (Thermo Scientific). Then the slides of sperm cells and cryosections of mouse testes were washed in 1 mL PBS and blocked in 10% donkey serum before being incubated overnight at 4°C with the following primary antibodies: rabbit polyclonal anti-TTC29 (PA5-70409, Invitrogen, 1:100), anti-TTC30A (sc-393206, Santa Cruz Biotechnology, 1:100), anti-IFT52 (17534-1-AP, Proteintech, 1:100), anti-α-tubulin antibody (EP1332Y, abcam, 1:500), and monoclonal mouse anti-α-tubulin (T9026, Sigma, 1:500). Washes were performed using PBS with 0.1% (v/v) Tween20, followed by 1 h incubation at room temperature with highly cross-absorbed secondary antibodies Alexa Fluor 488 anti-Mouse IgG (34106ES60, Yeasen, 1:1000) and Cy3-conjugated AffiniPure Goat Anti-Rabbit IgG (111-165-003, Jackson, 1:4000). Images were captured with a confocal microscope (Zeiss LSM 880).

Mouse Model Generation Using CRISPR-Cas9

The frameshift mutations in *Ttc29* were generated in mice by using CRISPR-Cas9 technology according to previous studies.[37–39] The single-guide RNA (sgRNA) was specifically designed against

Table 1. Semen Characteristics and Sperm Morphology in the Men Carrying Bi-allelic *TTC29* Mutations

-	Human Subject			
-	A002 IV-1	A038 IV-1	S003 II-1	Reference Limits
Semen Parameters				
Semen volume (mL)	4.5	2.5	3.0	1.5[a]
Sperm concentration (10^6/mL)	9.0	57.6	39.5	15.0[a]
Motility (%)	1.3	0.0	0.8	40.0[a]
Progressive motility (%)	0.0	0.0	0.0	32.0[a]
Sperm Morphology				
Normal flagella (%)	16.0	0.0	5.0	23.0[b]
Absent flagella (%)	17.5	5.5	12.0	5.0[b]
Short flagella (%)	39.5	63.5	36.5	1.0[b]
Coiled flagella (%)	26.0	26.5	33.0	17.0[b]
Angulation (%)	1.0	4.5	2.0	13.0[b]
Irregular caliber (%)	0.0	0.0	11.5	2.0[b]
Flagellar Ultrastructural Abnormality[c]				
Abnormal mid-piece (%)	80.0	86.6	81.8	11.8 (8.6–15.1)[d]
Abnormal end piece (%)	92.1	87.5	75.1	8.1 (5.2–11.2)[d]

[a]Reference limits according to the WHO standards.[62]
[b]Reference limits according to the distribution range of morphologically normal spermatozoa observed in 926 fertile individuals.[63]
[c]More than one hundred cross sections were analyzed.
[d]Values represent the mean (range) and are from the statistics of more than three healthy and fertile individuals in this study.

mouse chr8:78333554–78333613 (GRCm38/mm10) at *Ttc29* exon 12 according to the position of *TTC29* stop-gain variant p.Tyr369* , which was shared by two human subjects, A002 IV-1 and S003 II-1, of this study. In brief, the sgRNAs were synthesized, annealed, and ligated to the pX458 plasmid, which had been digested with *Bbs*I. Then the pX458 plasmid harboring corresponding sgRNA was transfected into embryonic stem cells which were separated with flow cytometry and plated on dishes 24 h later. Single colonies were picked out and expanded for genotyping. Then the embryonic stem cells carrying genetic modifications were injected into blastocysts, which were generated by mating superovulated female mice with wild-type (WT) C57BL/6 male mice. After a short *in vitro* culture, the injected blastocysts were transferred into pseudopregnant female mice. The frameshift mutation in *Ttc29* was identified in founder mice and their offspring through the use of PCR and Sanger sequencing. All animal experiments were carried out in accordance with the recommendations of the US National Institutes of Health's Guide for the Care and Use of Laboratory Animals. This study was approved by the animal ethics committee at the School of Life Science, Fudan University. Adult mice (aged 6 weeks or older) were used in this study.

In Vitro Fertilization and Intracytoplasmic Sperm Injection

Two-month-old B6D2F1 (C57BL/6 × DBA2) female mice were superovulated as previously described.[40] In brief, the female mice were superovulated by injecting 5–7.5 IU of pregnant mare serum gonadotropin (PMSG), followed by 5–7.5 IU of human chorionic gonadotropin (hCG) 48 h later. For IVF, sperm samples were collected from epididymis and added into the human tubal fluid (HTF; Millipore, Cat. # MR-070-D) drop. Then cumulus-intact oocytes, collected from superovulated females, were transferred into the sperm-containing HTF drop. After 5–6 h of incubation, the embryos were washed in HTF and transferred into KSOM medium (Millipore, Cat. # MR-106-D) to further culture at 37°C under 5% CO_2. Fertilization rates were evaluated by recording the numbers of two-cell embryos and late-stage blastocysts at 20 h and 91 h later, respectively.

For ICSI, oocytes were obtained from superovulated females, and sperm heads were injected into oocytes through the use of a Piezo-driven pipette as previously described.[41] Then the injected oocytes were cultured in KSOM medium at 37°C under 5% CO_2. Two-cell embryos and blastocysts were counted 20 h and 96 h later, respectively.

Results

Identification of Bi-allelic Truncating Mutations of *TTC29* in MMAF-Affected Men

In this study, high-throughput exome sequencing and bioinformatic analyses were performed on 80 MMAF-affected men according to our previously described protocol.[14] We identified bi-allelic truncating mutations of *TTC29* (GenBank: NM_031956.3) in three (3.8%) unrelated cases of 80 MMAF-affected men (Figure 1A, Table S1). These *TTC29* truncating mutations were further verified through Sanger sequencing (Table S2) and illustrated in Figure 1A. *TTC29* is located on the human chromosome 4, and it contains 13 exons which encode a predicted 475-amino-acid protein (NCBI: NP_114162.2; UniProt: Q8NA56). TTC29 protein contains tetratricopeptide repeat (TPR) domains, and

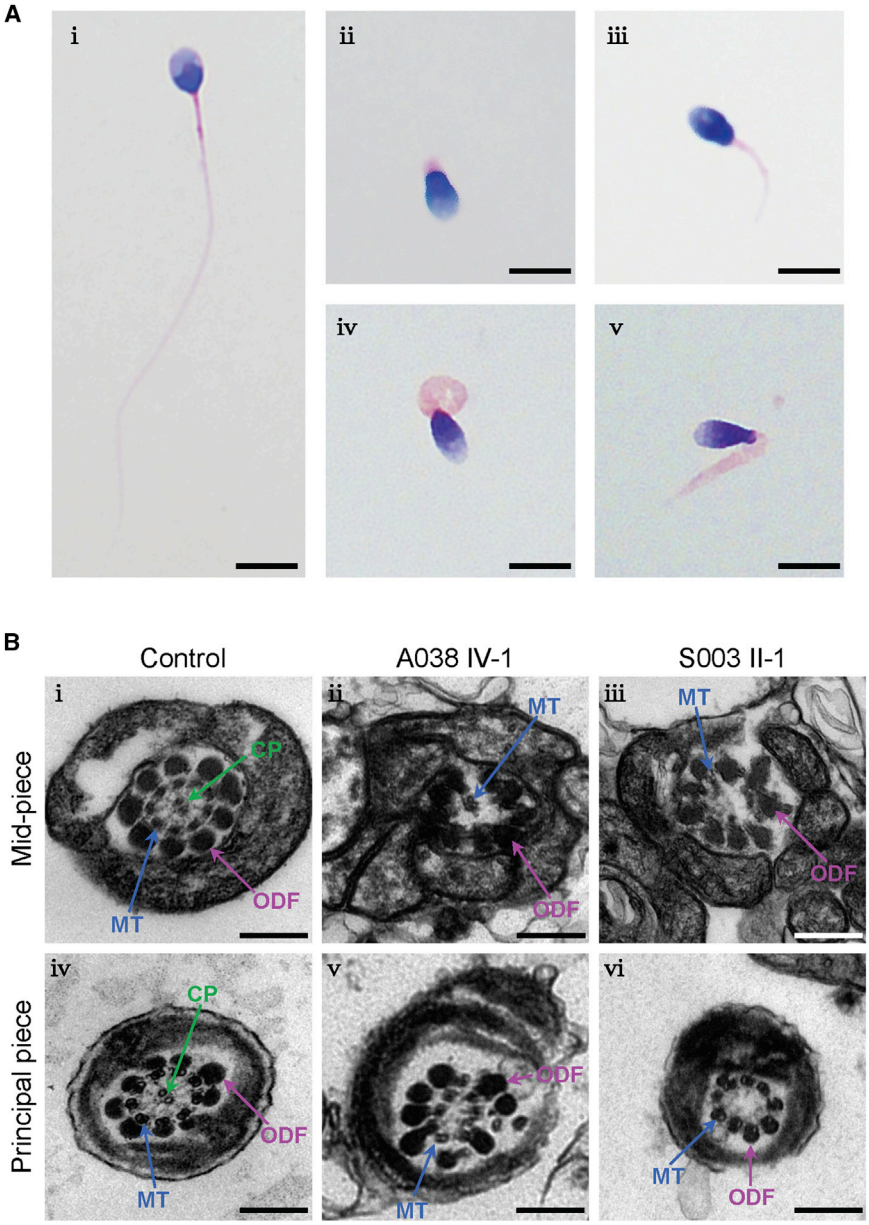

Figure 2. Sperm Morphology and Ultrastructure Analyses for Men Harboring *TTC29* Mutations

(A) Light microscopy analysis of spermatozoa from the control (i) and men harboring *TTC29* mutations (ii–v). Most spermatozoa from men harboring *TTC29* mutations have flagella that are absent (ii), short (iii), coiled (iv), or of irregular caliber (v). The spermatozoa from subject A038 IV-1 are given as examples of typical MMAF phenotypes observed in men harboring *TTC29* mutations. Scale bars: 5 μm

(B) TEM analyses of sperm cells from a fertile control and two men harboring *TTC29* mutations. Cross-sections of the mid-piece (i) and principal piece (iv) of the flagella in a control man show the typical "9 + 2" microtubule structure, including nine peripheral microtubule doublets paired with nine outer dense fibers and the central pair of microtubules, surrounded by the organized mitochondrial sheath or fibrous sheath. The ultrastructure observed in cross sections of the flagella in men harboring *TTC29* mutations indicates the misarranged outer dense fibers (ii) and disorganization of the peripheral microtubules with lack of the central pair of microtubules (iii, v, and vi). Scale bars: 200 nm. Abbreviations: CP, central pair of microtubules (green arrows); MT, peripheral microtubule doublet (blue arrows); ODF, outer dense fiber (purple arrows).

TTC29 protein is preferentially expressed in the human testis according to the data from the Encyclopedia of DNA Elements (ENCODE), the Functional Annotation of the Mammalian Genome (FANTOM), and the Genotype Tissue Expression (GTEx) project.

In consanguineous family A002, a homozygous stop-gain mutation of *TTC29* (c.1107C>G [p.Tyr369*]) was identified in proband A002 IV-1, and this variant was inherited from his heterozygous parental carriers (Figure 1A). Furthermore, a homozygous frameshift mutation in *TTC29* (c.412_425del [p.Asp138Leufs*10]) was identified in proband IV-1 from consanguineous family A038 (Figure 1A). Both of these *TTC29* truncating mutations in two consanguineous families introduce premature stop codons and are consequently expected to induce nonsense-mediated mRNA decay that can affect protein synthesis.

Notably, the *TTC29* c.1107C>G (p.Tyr369*) variant was recurrently identified in another unrelated family, S003 (Figure 1A), in which the mother transmitted a *TTC29* c.1107C>G (p.Tyr369*) allele to the proband. Furthermore, a *TTC29* splice-site variant, c.977+1G>T, was identified at the paternal allele in proband S003 II-1 (Figure 1A). According to the Human Splicing Finder (HSF), the *TTC29* c.977+1G>T variant abrogates the consensus donor site, leading to altered splicing and subsequent frameshift. To further investigate the predicted alteration of gene splicing, reverse-transcription PCR (RT-PCR) was performed with the cDNA reversely transcribed from sperm RNA (Table S3). The RT-PCR product obtained from proband S003 II-1 displayed two bands; one had the same length (455 bp) with the control, but the other was short (363 bp), suggesting a splicing alteration (Figure S1A). Sanger sequencing of cDNA indicated the skipping of *TTC29* exon 9 at the mutated allele (Figure S1B). Therefore, the *TTC29* c.977+1G>T variant in the canonical donor site of intron 9 was predicted to lead to a subsequent frameshift (p.Ser326Profs*8) secondary to skipping of exon 9 (Figure S1C).

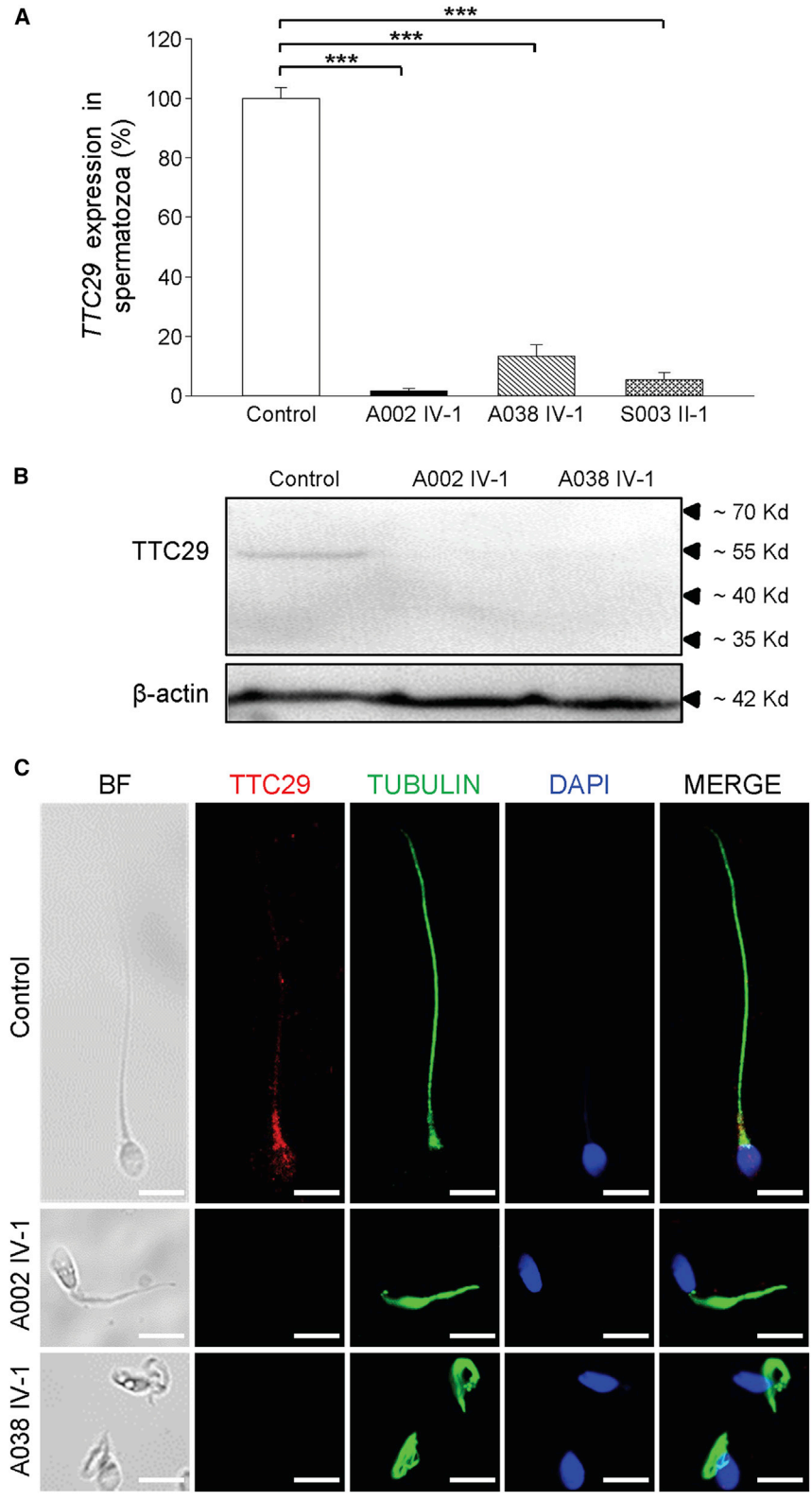

Figure 3. Expression Analysis of *TTC29* mRNA and Location of TTC29 Protein in Sperm Flagella

(A) The expression of *TTC29* mRNA in the spermatozoa from a normal control and men harboring *TTC29* mutations. RT-qPCR assays suggested that the level of *TTC29* mRNA was reduced significantly in the sperm from men harboring *TTC29* mutations when compared to the level in sperm from a normal control man. Data represent the means ± standard error of the means (SEM) of three independent experiments. Two-tailed Student's paired or unpaired t tests were used as appropriate. ***$p < 0.001$.

(B) Immunoblotting analysis of TTC29 protein in sperm lysates from a normal control and from men harboring *TTC29* mutations (A002 IV-1 and A038 IV-1). β-actin was used as a loading control.

(C) TTC29 immunostaining in human spermatozoa from a normal control and from men harboring *TTC29* mutations. Sperm cells were stained with anti-TTC29 (red) and anti-α-tubulin (green) antibodies. DNA was counterstained with DAPI as a nuclei marker. TTC29 staining is concentrated at the base of sperm flagella and faintly along flagella in the fertile control but is almost absent in the sperm flagella of men harboring *TTC29* mutations. Scale bars: 5 μm.

atospermia according to semen characteristics (Table 1). Notably, no spermatozoa with progressive motility were observed in any subjects affected by bi-allelic truncating mutations of *TTC29*. The morphology of the sperm cells was assessed with H&E staining and SEM. More than 80% of the spermatozoa from men harboring *TTC29* mutations displayed abnormal flagella (Table 1). Subject A038 IV-1 with the early truncating mutation of *TTC29* (c.412_425del [p.Asp138Leufs*10]) had a higher malformation rate of sperm flagella than those of the other two subjects with late truncating mutations of *TTC29*. When compared with the long and thin tails in the normal spermatozoa from a healthy control man, the spermatozoa from men harboring *TTC29* mutations displayed obvious MMAF phenotypes, including short, absent, coiled flagella and irregular caliber (Figures 2A and S2).

TEM was conducted according to a previously described protocol[14] to further investigate sperm flagellar ultrastructure in the subjects with *TTC29* mutations. Higher rates of abnormal flagellar ultrastructures were detected in men

Asthenoteratospermia Phenotypes in Men Harboring *TTC29* Mutations

Semen analysis was conducted in the source laboratories during routine examination of the individuals according to WHO guidelines.[42] All men harboring *TTC29* mutations were shown to have severe-to-complete asthenoter-

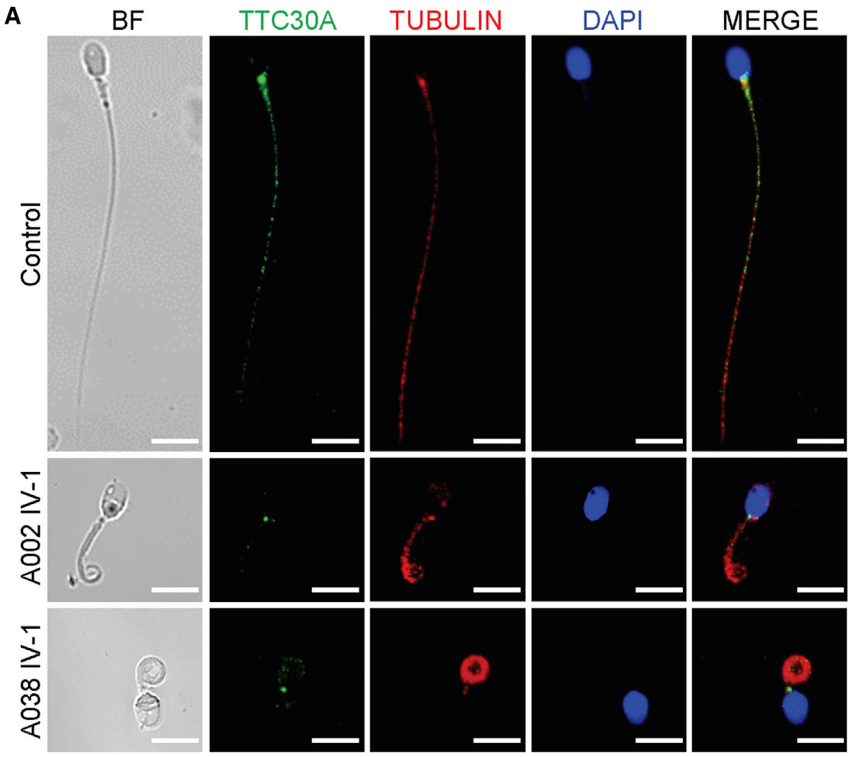

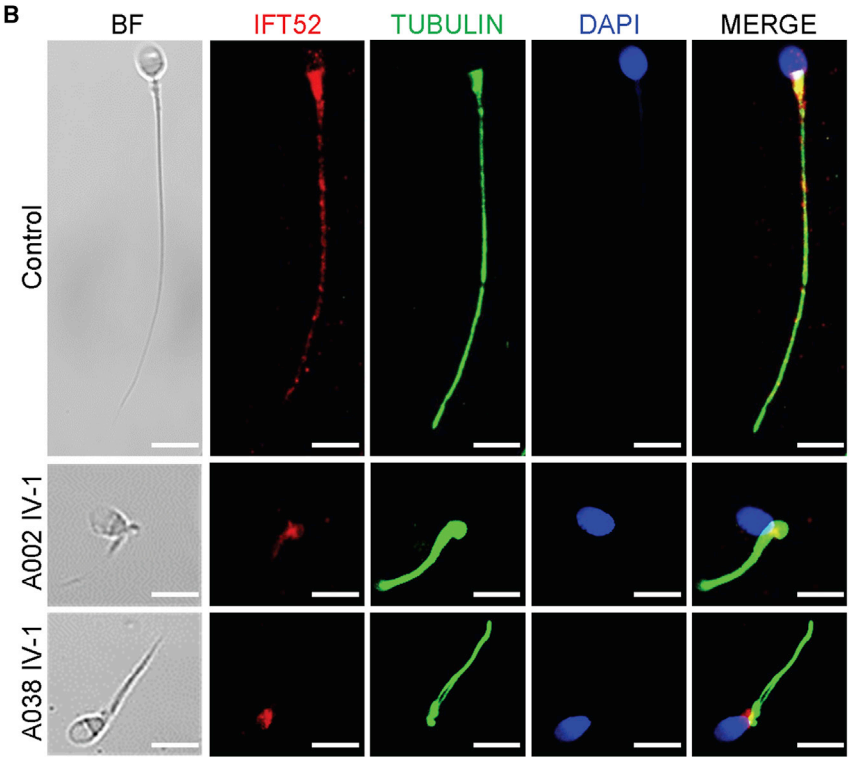

Figure 4. Affected TTC30A and IFT52 Immunostaining in the Spermatozoa from Men Harboring *TTC29* Mutations

(A) Sperm cells from a normal control and from men harboring *TTC29* mutations were stained with anti-TTC30A (green, a component of IFT complex B) and anti-α-tubulin (red) antibodies. DNA was counterstained with DAPI as a nuclei marker. In spermatozoa from the fertile control, TTC30A staining appears to be located mainly in the basal body and lightly decorates the sperm flagellum. In the sperm cells from men harboring *TTC29* mutations, TTC30A staining is strongly reduced or totally absent. Scale bars: 5 μm.

(B) Sperm cells from a normal control and from men harboring *TTC29* mutations were stained with anti- IFT52 (red, a key component of the IFT-B complex) and anti-α-tubulin (green) antibodies. DNA was counterstained with DAPI as a nuclei marker. IF52 staining was found mainly at the base of the flagellum and faintly along cilia in control spermatozoa but revealed weak staining and only aggregated at the base of sperm flagella in men harboring *TTC29* mutations. Scale bars: 5 μm.

harboring *TTC29* mutations when compared with those in fertile individuals (Table 1). The cross sections displayed the typical "9 + 2" microtubule structure (nine peripheral microtubule doublets and a central pair of microtubules) in sperm flagella from a control specimen, but presented a dramatic disorganization in axonemal or other peri-axonemal structures in the spermatozoa from men harboring *TTC29* mutations (Figure 2B). For example, the unassembled outer dense fibers (ODFs) were found at the mid-piece of sperm flagella, and the absent (9 + 0 conformation) or misplaced central-pair microtubules were also constantly observed in the sections of the principal piece (Figure 2B).

Deficiency of TTC29 and Abnormal Intraflagellar Transport

To investigate pathogenicity of the MMAF-associated *TTC29* mutations, we newly obtained the sperm samples from a fertile control man and from men harboring *TTC29* mutations. The expressions of *TTC29* mRNA and protein were investigated using real-time quantitative PCR (RT-qPCR) and immunoblot assays, respectively. It was shown that the expression of *TTC29* mRNA in sperm was reduced dramatically in men harboring *TTC29* mutations when compared to the control (Figure 3A). Immunoblotting analysis of control sperm lysates through the use of a commercial antibody against TTC29 detected a band of ~55 Kd (Figure 3B), which is consistent with the predicted molecular weight of the protein encoded by the longest *TTC29* transcript (Ensembl: ENST00000513335.5). The corresponding band was absent when we investigated the

Table 2. Semen Characteristics, Ultrastructural Abnormalities, and Sperm Morphology in the *Ttc29*-Mutated Male Mice

-	WT Male Mice[a]	*Ttc29*-Mutated Male Mice[a]
Semen Parameter[b]		
Sperm concentration (10^6/mL)	19.1 (15.7–21.7)	12.8 (8.9–18.0)
Motility (%)	81.8 (81.0–82.6)	51.2 (3.0–71.0)*
Progressive motility (%)	65.8 (64.0–67.0)	39.6 (2.0–57.0)*
Sperm Morphology		
Absent flagella (%)	4.3 (2.5–6.1)	5.7 (2.0–12.1)
Short flagella (%)	3.0 (2.4–3.6)	4.6 (1.5–9.5)
Coiled flagella (%)	0.8 (0.6–1.1)	0.9 (0.5–2.5)
Irregular caliber (%)	2.3 (2.0–3.2)	1.4 (0.6–2.7)
Bent flagella (%)	2.8 (0.5–5.4)	6.3 (2.5–16.1)***
Flagellar Ultrastructural Abnormality[c]		
Abnormal mid-piece (%)	2.7 (2.1–3.3)	14.0 (8.0–23.5)**
Abnormal end piece (%)	3.1 (1.8–4.4)	32.7 (11.4–55.0)***

* $p < 0.05$, ** $p < 0.01$, *** $p < 0.001$. The items with statistical significance are shown in bold.
[a]Values represent the mean (range).
[b]Per single epididymis.
[c]More than one hundred cross sections were analyzed.

sperm from men harboring *TTC29* mutations (Figure 3B). Our experimental observations on *TTC29* expression revealed the possibility of nonsense-mediated mRNA decay triggered by premature translation termination.

To determine the localization of TTC29 in normal spermatozoa and the effect of TTC29 deficiency on the assembly and/or anchorage of axonemal protein complexes, immunofluorescence (IF) analysis was performed with anti-TTC29 and other antibodies targeting proteins located to various axonemal and peri-axonemal structures of the sperm flagella. We observed that TTC29 immunostaining was localized mainly at the base of sperm flagella and faintly along flagella in normal spermatozoa, but it was almost absent in the spermatozoa from men harboring *TTC29* mutations (Figures 3C and S3). Additionally, the analysis on TTC30A (also known as IFT70A, a component of IFT complex B), which is essential for anterograde IFT and ciliogenesis,[43,44] revealed a significantly reduced TTC30A staining in the spermatozoa from men harboring *TTC29* mutations (Figures 4A and S4). Furthermore, IFT52 (a key component of IFT complex B), which plays a crucial role in microtubule anchorage and centrosome cohesion,[45,46] showed an atypical localization on the sperm flagella of men harboring *TTC29* mutations in comparison with the control. IFT52 staining was found mainly at the flagellar base and faintly along flagella in the control, but it was weak and only aggregated at the base of sperm flagella in men harboring *TTC29* mutations (Figures 4B and S5). These findings indicated the *TTC29*-associated abnormal assembly of anterograde complex in IFT.

Ttc29-Mutated Male Mice Resembled Asthenoteratospermia Phenotypes

Ttc29-mutations in mice were constructed using the CRISPR-Cas9 system[37–39] to further investigate the roles of *TTC29* in sperm flagellar formation. Sanger sequencing of *Ttc29* homozygous mutated mice confirmed the presence of a frameshift mutation (c.1128del), which was predicted to cause premature translational termination (p.Phe377Serfs*11) (Figure S6, Table S4). RT-qPCR assay (Table S5) was performed to compare the level of *Ttc29* transcription in the spermatozoa of WT, heterozygous carrier ($Ttc29^{+/mut}$) and *Ttc29*-mutated ($Ttc29^{mut/mut}$) male mice. As expected, the level of *Ttc29* mRNA was significantly lower in $Ttc29^{mut/mut}$ male mice than in WT male mice, indicating a partial nonsense-mediated mRNA decay triggered by premature translational termination (Figure S7A). Immunoblotting assay revealed the near absence of Ttc29 protein in the spermatozoa from $Ttc29^{mut/mut}$ male mice compared to the WT male mice, and the expression of Ttc29 protein in epididymal spermatozoa from WT male mice was lower than that in mouse testis (Figures S7B and S8). Consistently, IF analysis was also performed on the spermatozoa and testicular sections from $Ttc29^{mut/mut}$ and WT male mice with TTC29 antibody described above. The TTC29 immunostaining was almost absent in the spermatozoa and testes from $Ttc29^{mut/mut}$ male mice, further suggesting a low level of TTC29 protein (Figures S9 and S10). Furthermore, the expression and location of Ttc30a1 (an ortholog of human TTC30A in mouse) and Ift52 were also analyzed in the spermatozoa and testicular sections from WT and $Ttc29^{mut/mut}$ male mice. Ttc30a1 and Ift52 immunostaining were both located in the mid-piece of sperm flagella or weakly along flagella from both WT and *Ttc29*-mutated male mice (Figures S11 and S12). For testicular sections, Ttc30a1 and Ift52 immunostaining were mainly concentrated in the elongating spermatids in testicular sections from WT and *Ttc29*-mutated male mice (Figures S13 and S14).

Semen characteristics, sperm morphology, and ultrastructure were investigated in *Ttc29*-mutated male mice. Notably, sperm motility was significantly reduced in $Ttc29^{mut/mut}$ male mice when compared to that of WT male mice (Table 2). In particular, a significantly lower rate of sperm progressive motility and a significantly higher rate of immotility were observed in $Ttc29^{mut/mut}$ male mice when compared with WT male mice (Figure S15A). Additionally, three kinematic parameters for sperm velocity, including curvilinear velocity (VCL), straight-line velocity (VSL), and average-path velocity (VAP), were significantly reduced in $Ttc29^{mut/mut}$ male mice when compared with WT male mice (Figure S15B). There seems to be no significant difference between WT and $Ttc29^{mut/mut}$ male mice in flagellar beating assessed based on beat/cross frequency (BCF). Also, no significant difference in testis weight was observed between WT and $Ttc29^{mut/mut}$ male mice (Figure S16). Light microscopy revealed a higher rate of bent flagella in $Ttc29^{mut/mut}$ male mice than in wild type (Table 2, Figure S17). Furthermore, TEM observations on

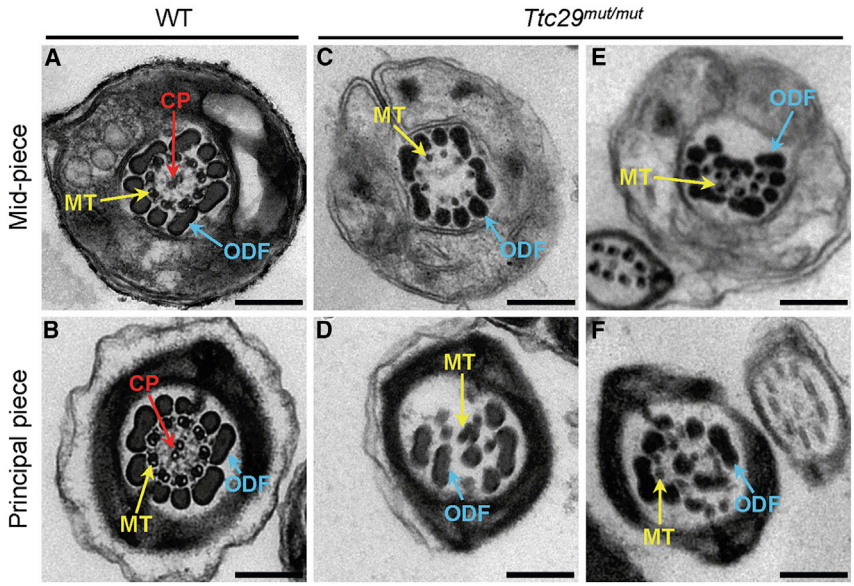

Figure 5. TEM Cross-Sections of Spermatozoa from *Ttc29*$^{mut/mut}$ Male Mice Reveal Multiple Structural Axonemal Defects

(A) Cross-sections of the mid-piece of sperm flagellum in a WT male mouse. The axoneme is composed of nine peripheral microtubules doublets and a central pair of singlet microtubules, surrounded by nine outer dense fibers and the mitochondrial sheath.

(B) Cross-sections of the principal piece of sperm flagellum from a WT male mouse. Typical "9 + 2" microtubule structure was observed and surrounded by outer dense fibers and the fibrous sheath.

(C–F) Various axonemal anomalies can be observed, including the lack of the central pair of microtubules (C, D) or randomly oriented outer dense fibers (E, F).

Abbreviations: CP, central pair of microtubules (red arrows); MT, peripheral microtubule doublet (yellow arrows); ODF, outer dense fiber (blue arrows); WT, wild type. Scale bars: 200 nm.

flagellar ultrastructure of the spermatozoa from mouse cauda epididymis revealed the lack of central-pair microtubules or the ODF disorganization in *Ttc29*$^{mut/mut}$ male mice (Figure 5). The rates of spermatozoa with abnormal flagellar ultrastructure were significantly higher in *Ttc29*$^{mut/mut}$ male mice when compared with that in WT male mice (Table 2).

Damaged Fertility and Poor Outcomes of IVF in *Ttc29*-Mutated Male Mice

To assess the fertility and reproductive behavior of *Ttc29*-mutated mice, the WT and *Ttc29*-mutated male mice (6 weeks of age or older) were mated to similarly aged WT females, and the numbers of pups per litter were counted. Notably, the average number of pups per litter (0–2 litters produced per female over 3 months, 2.50 ± 2.81 pups per litter) in *Ttc29*$^{mut/mut}$ male mice was significantly less than that in WT male mice (3–4 litters produced per female over 3 months, 7.33 ± 0.13 pups per litter) during 3 months of breeding (Figure S18). No obvious difference in fertility was observed between *Ttc29*$^{mut/mut}$ female mice and WT females when mated with WT male mice (Figure S18).

IVF was also performed as described in previous studies[47,48] to further investigate the fertility of *Ttc29*-mutated male mice. Notably, rates of both two-cell embryos and blastocysts were significantly lower in *Ttc29*$^{mut/mut}$ male mice than in WT male mice (Figure 6A). Our IVF findings strongly suggest that *TTC29* plays an important role in sperm quality and male fertility.

Good Prognosis of ICSI in Men Harboring *TTC29* Mutations and *Ttc29*-Mutated Male Mice

A previous study revealed that MMAF-affected men with *DNAH1* mutations have a good clinical outcome following ICSI.[49] To examine whether the male infertility induced by *TTC29* mutations could also be overcome by ICSI treatment, we performed ICSI for *Ttc29*-mutated male mice according to a previously described method.[41] As expected, the rates of two-cell embryos and blastocysts in *Ttc29*$^{mut/mut}$ male mice were almost equivalent to those in WT male mice (Figure 6B). Our experimental observations indicated that the male subfertility in *Ttc29*-mutated mice could be overcome by ICSI. Therefore, we speculated that ICSI might also be applicable to the patients with *TTC29*-associated MMAF.

Coincidentally, the three men harboring *TTC29* mutations in this study had undergone assisted reproductive therapy by ICSI and acquired good clinical outcomes. As shown in Table 3, the overall rates (median) of fertilization, cleavage, eight-cell formation, and blastocyst formation after ICSI were 74.1%, 100.0%, 40.9%, and 31.8%, respectively. We compared the *TTC29*-mutated group with the age-matched control group with oligoasthenoteratozoospermia (OAT) and with the *DNAH1*-mutated MMAF group that had been known to have successful ICSI clinical outcomes.[49] There were no statistically significant differences in rates of fertilization, cleavage, 8-cell formation, blastocyst formation, implantation, and clinical pregnancy between the *TTC29*-mutated group and either the *DNAH1*-mutated group or the OAT controls (Table 3). Our findings suggest that *TTC29*-associated MMAF and male subfertility can be treated by ICSI.

Discussion

As mentioned above, we identified bi-allelic truncating mutations of *TTC29* in three (3.8%) unrelated cases of 80 MMAF-affected men, and this result cannot be explained by any known MMAF-associated genes. Notably, all of these *TTC29* variants are novel and absent from human population genome datasets archived in the 1000 Genomes Project, Exome Aggregation Consortium (ExAC), and Genome Aggregation Database (gnomAD)

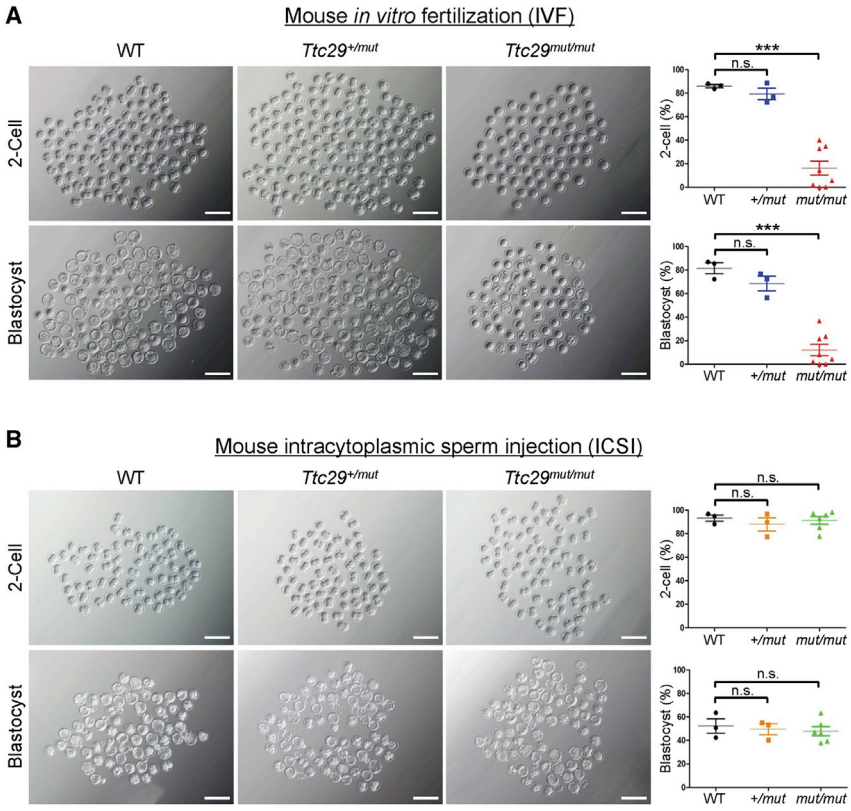

Figure 6. Impaired Fertilization Capability by Loss of Ttc29 Function Could Be Rescued by Intracytoplasmic Sperm Injection

(A) Representative two-cell embryos and blastocysts from *in vitro* fertilization. Scale bar, 200 μm. The two-cell rates and blastocyst rates were counted after caudal epididymal sperm fertilized oocytes that were collected from superovulated wild-type (WT) females. Here, the blastocyst rates were shown as the percentage of blastocysts out of total oocytes. The WT, $Ttc29^{+/mut}$, and $Ttc29^{mut/mut}$ groups consisted of three, three, and eight male mice, respectively. A total of 1,305 embryos were counted. Data are represented as means ± SEM; ***$p < 0.001$. Abbreviations: n.s., not significant; WT, wild type.

(B) Representative two-cell embryos and blastocysts from intracytoplasmic sperm injection. Scale bar, 200 μm. The two-cell rates and blastocyst rates were counted after sperm heads of *Ttc29*-mutated male mice were injected into oocytes that were collected from superovulated wild-type (WT) females. Here, the blastocyst rates were shown as the percentage of blastocysts out of total injected oocytes. The WT, $Ttc29^{+/mut}$, and $Ttc29^{mut/mut}$ groups consisted of three, three, and six male mice, respectively. A total of 759 embryos were counted. Data are represented as means ± SEM. Abbreviations: n.s., not significant; WT, wild type.

(Table S1). Through functional experiments, the absence of TTC29 was observed in the spermatozoa of men harboring *TTC29* mutations. Therefore, the MMAF phenotypes in these Chinese men are likely to be explained by the bi-allelic mutations in *TTC29*. Intriguingly, *TTC29* mutations were also newly identified in MMAF-affected individuals of African and Iranian origins (Lores et al., a related manuscript in press at the *American Journal of Human Genetics*).

TTC29 is an evolutionarily conserved and TPR-domain-containing protein. The TPR domain contains many repeated motifs that form structural domains in proteins, and these structural domains can act as interaction scaffolds in the formation of multi-protein complexes involved in numerous cellular processes.[50] Previous studies also indicated that TPR family proteins could play an important role in cilia- and flagella-associated functions. For example, IFT88 is important for primary cilia assembly in mammals, and the defects in mouse *Ift88* (also known as *TPR repeat protein 10*) can lead to polycystic kidney disease.[51] Our recent study reported that bi-allelic mutations in *TTC21A*, which encodes a member of the TPR family, induced asthenoteratospermia in both humans and mice.[14] All of these studies remind us of the important role of TPR-domain-containing proteins in the assembly of cilia and flagella. The TPR domains are required for proper localization of TTC29 into the axoneme in *Trypanosoma brucei* (Lores et al., a related manuscript in press at *American Journal of Human Genetics*). In our study, all of the MMAF-associated truncating mutations of *TTC29* are located at or before the TPR domains, leading to the damage of TPR domains in TTC29 protein (Figure 1B). Consistently, our RT-qPCR, immunoblotting, and IF assays also revealed the significantly reduced expression of TTC29 at mRNA and protein levels in the spermatozoa of men harboring *TTC29* mutations (Figure 3). Therefore, it is speculated that deficiency of TPR domains contained in TTC29 protein may be an important factor for MMAF phenotypes.

IFT is a conserved mechanism essential for the assembly and maintenance of most eukaryotic cilia and flagella, and it has a bi-directional protein transport system inside cilia. Anterograde transport, which is regulated by IFT complex B, carries ciliary components from the cell body to the tip of cilia, while retrograde transport is regulated by IFT complex A and sends the products of turnover back to the cell body from cilia.[20,21,52,53] Previous studies reported that IFT complex B plays a major role in the assembly and maintenance of cilia and flagella.[21,54] In most cases, mutations or knockdown of IFT complex B proteins result in absent or very short cilia or flagella.[51,55–58] For example, the mice with a homozygous *Ift20* mutation displayed significantly reduced sperm counts, significantly reduced motility, and even abnormally shaped spermatid heads.[58] Here we identified TTC29, a potential member of IFT complex B,[43] as an asthenoteratospermia-associated protein. TTC29 was involved in functional interaction with the IFT machinery, and partial knockdown of Ttc29 in *Xenopus* multi-ciliated epithelial cells resulted in a significant decrease in the mean rate of anterograde IFT,[43] suggesting

Table 3. Clinical Outcomes of ICSI Cycles Using Spermatozoa of *TTC29*-Mutated, *DNAH1*-Mutated Men with MMAF and Controls

-	Group A	Group B	Group C	Comparisons of Three Groups		A versus B		A versus C		B versus C	
-	*TTC29*-Mutated MMAF	*DNAH1*-Mutated MMAF	OAT as Controls	*F*/*H* Value	*p*	Test Statistic	*p*	Test Statistic	*p*	Test Statistic	*p*
No. of couples	3	11	301	NA	NA	NA	NA	NA	NA	NA	NA
Mean male age (years)	31.7 ± 6.7	32.7 ± 4.7	30.1 ± 4.9	1.718	0.181	N/A	1.000	N/A	1.000	N/A	0.231
Mean female age (years)	27.3 ± 3.2	28.3 ± 4.2	28.4 ± 4.2	2.500	0.084	N/A	0.491	N/A	1.000	N/A	0.088
No. of ICSI cycles	3	11	301	NA	NA	NA	NA	NA	NA	NA	NA
No. of oocytes injected	11 (7,24)	10 (6, 20)	11(1, 34)	0.362	0.834	−0.472	1.000	−0.413	1.000	−0.435	1.000
Fertilization rate (%)	71.4 (63.6, 91.7)	63.6 (40.0, 86.0)	83.3 (12.5, 100.0) (3219/4077)	8.700	0.013	−0.707	1.000	−0.726	1.000	−2.872	0.012*
Cleavage rate (%)	100.0 (80.0, 100.0)	100.0 (70.0, 100.0)	100.0 (66.7, 100.0) (3188/3219)	4.455	0.108	−0.091	1.000	−0.966	1.000	−1.909	0.168
8-cell formation rate (%)	40.9 (0, 85.7)	57.1(0, 100.0)	70.6 (10.5, 100.0)	2.859	0.239	−1.101	0.873	−1.349	0.531	−1.031	0.909
Blastocyst formation rate (%)	31.8 (0, 57.1)	53.5 (0, 100.0)	60.0 (0, 100.0)	4.979	0.083	−1.018	1.000	−1.882	0.180	−1.232	0.654
No. of transfer cycles	2	9	301	NA	NA	NA	NA	NA	NA	NA	NA
Number of embryos transferred per cycle	1 (0, 2)	2 (0,3)	2 (1, 2)	1.993	0.369	−0.742	1.000	−1.368	0.513	−0.421	1.000
Implantation rate (%)	66.7 (2/3)	31.3 (5/16)	47.9 (229/478)	NA	NA	N/A	0.592[b]	0.005	0.945[a]	1.723	0.190
Clinical pregnancy rate per transfer cycle (%)	100.0 (2/2)	55.6 (5/9)	57.1 (172/301)	NA	NA	0.136	0.712[a]	0.254	0.614[a]	0.061	0.805[a]
Miscarriage rate (%)	0 (0/2)	20.0 (1/5)	11.6 (20/172)	NA	NA	NA	NA	N/A	NA	N/A	0.945[b]

Symbols: NA, not available data or not being compared; N/A, not applicable, statistical analysis was performed by Fisher's exact test and thus without the Chi-square value; *, the corrected inspection level, α of 0.0167 was used to analyze pairwise comparisons among three groups for categorical data.
Annotations: A versus B, group A compared with group B; A versus C, group A compared with group C; B versus C, group B compared with group C; OAT, oligoasthenoteratozoospermia; F, statistics of ANOVA; H, statistics of Kruskal-Wallis test.
Statistical analyses were performed by an independent statistician blinded to clinical outcomes. Descriptive statistics were expressed using mean ± standard deviation for normally distributed variables. ANOVA was used for measurement data. The Chi-square test or Fisher's exact test was performed to analyze categorical data. The non-normal distributed variables were shown with median (min, max) and analyzed with independent-samples Kruskal-Wallis test. All the tests were performed using a two-sided test of difference where the inspection level α of 0.05 and a difference with $p < 0.05$ were considered statistically significant. Pairwise comparisons among the three groups were corrected by Bonferroni method for measurement data.
[a]Yate's corrected Chi-square test
[b]Fisher's exact test

the association of Ttc29 with components of the anterograde IFT-B complex. Furthermore, SPAG6, a component of the central pair complex, was almost absent in the sperm flagella from men harboring *TTC29* mutations, indicating the impact of TTC29 protein on the positioning of axonemal proteins (Lores et al., a related manuscript in press at *American Journal of Human Genetics*). Coincidentally, our analyses of sperm morphology and ultrastructure displayed serious defects in external morphology and internal ultrastructure of spermatozoa from men harboring *TTC29* mutations and *Ttc29*-mutated mice, defects which may be caused by failed anterograde IFT.

Furthermore, we also investigated the effect of *TTC29* mutations on human TTC30A and IFT52, two members of IFT complex B. A significantly reduced TTC30A staining was observed in the spermatozoa from men harboring *TTC29* mutations, and this result further supports the predicted linkage of TTC29 to TTC30A by bioinformatic analysis in a previous study.[43] Furthermore, IFT52 staining only aggregated at the base of sperm flagella in men harboring *TTC29* mutations, and was weaker than that in the control subject as well. Coincidentally, a recent study demonstrated that a robust interaction of IFT70A (TTC30A) with IFT52–IFT88 dimer in the IFT-B complex is required for ciliogenesis.[44] Therefore, all of these previous reports and our findings in this study jointly revealed the participation of TTC29 (as a potential member of IFT-B complex) in anterograde IFT.

TTC30A and IFT52 staining on the sperm and testis samples from *Ttc29*-mutated male mice seem not to be impacted by the deficiency of mouse Ttc29; this result is different from our experimental observations in humans. This difference may be due to the divergent protein interaction networks between human and mouse as predicted by the *in silico* tool String (Figure S19). The functional association between TTC29 and TTC30A was identified in human, but no supporting evidence was revealed in mouse. Therefore, TTC29/Ttc29 may participate in the IFT in different ways between human and mouse due to the evolutionarily divergent protein interaction networks. This may also be partially related to the difference in *TTC29*/*Ttc29*-associated phenotypic severities between

human and mouse. The observed morphological defects of sperm flagella from *Ttc29*-mutated male mice seem to be mildly impacted when compared with the severe flagella defects of men harboring *TTC29* mutations.

Assisted reproduction techniques (ART), such as IVF and ICSI, have become important tools for treating infertile couples.[59] For MMAF-associated asthenoteratospermia, no empirical medicinal treatment has been reported to improve the semen parameters; therefore, ICSI could be the only choice for the MMAF-affected cases.[60] However, previous studies suggested that MMAF cases caused by different mutations exhibit different prognoses following ICSI. For example, the patients with *DNAH1*-associated MMAF have good clinical outcomes following ICSI.[49] In contrast, a *CEP135*-associated MMAF subject had a failed pregnancy.[61] Therefore, comparative studies on ICSI outcomes between different MMAF-associated genes would be informative to clinicians before ART treatment recommendation. For ICSI treatment in this study, the rates of two-cell embryo and blastocyst in $Ttc29^{mut/mut}$ male mice are similar to those in WT male mice, suggesting that male subfertility of *Ttc29*-mutated mice could be overcome by ICSI. Coincidentally, all of the three men harboring *TTC29* mutations underwent ICSI with their own sperm, and the rates of fertilization, cleavage, eight-cell formation, and blastocyst formation were similar to those of the *DNAH1*-mutated group and OAT controls. The partners of two affected individuals (A002 IV-1 and S003 II-1) acquired successful clinical pregnancy. Therefore, our findings supported the contention that ICSI can be recommended for *TTC29*-associated asthenoteratospermia.

In conclusion, our genetic and functional analyses in human subjects and a mouse model strongly suggest that bi-allelic mutations of *TTC29* are a crucial genetic cause of MMAF-associated asthenoteratospermia. Furthermore, the effect of TTC29 deficiency on human TTC30A and IFT52 proteins indicated that TTC29 may participate in the anterograde IFT of flagella as a potential member of IFT-B complex. A good pregnancy outcome could be acquired through ICSI using the spermatozoa of men harboring *TTC29* mutations. Our study provides new knowledge to clinicians and genetic counselors for understanding the genetic etiology of asthenoteratospermia and male infertility.

Supplemental Data

Supplemental Data can be found online at https://doi.org/10.1016/j.ajhg.2019.10.010.

Acknowledgments

We would like to thank the families for participating and supporting this study. We also thank the Center of Cryo-electron Microscopy at Zhejiang University for technical support. This work was supported by National Natural Science Foundation of China (grant numbers 31625015, 31521003, and 81601340), Special Foundation for Development of Science and Technology of Anhui Province (2017070802D150), Jiangsu Commission of Health (H2018050), Foundation of the Education Department of Anhui Province (KJ2016A370), Shanghai Medical Center of Key Programs for Female Reproductive Diseases (2017ZZ01016), and Shanghai Municipal Science and Technology Major Project (2017SHZDZX01).

Declaration of Interests

The authors declare no competing interests.

Received: July 1, 2019
Accepted: October 11, 2019
Published: November 14, 2019

Web Resources

1000 Genomes Project, https://www.internationalgenome.org
ENCODE, https://www.encodeproject.org
Ensembl, http://www.ensembl.org
ExAC Browser, http://exac.broadinstitute.org
FANTOM, http://fantom.gsc.riken.jp
gnomAD, https://gnomad.broadinstitute.org
GTEx, https://www.gtexportal.org/home/
HUGO Gene Nomenclature Committee, https://www.genenames.org/
Human Protein Atlas, https://www.proteinatlas.org
Human Splicing Finder, http://www.umd.be/HSF3/
OMIM, https://www.omim.org
PolyPhen-2, http://genetics.bwh.harvard.edu/pph2/
SIFT, https://sift.bii.a-star.edu.sg
UCSC Genome Browser, http://genome.ucsc.edu
UniProt, https://www.uniprot.org

References

1. Tournaye, H., Krausz, C., and Oates, R.D. (2017). Novel concepts in the aetiology of male reproductive impairment. Lancet Diabetes Endocrinol. *5*, 544–553.
2. Robay, A., Abbasi, S., Akil, A., El-Bardisi, H., Arafa, M., Crystal, R.G., and Fakhro, K.A. (2018). A systematic review on the genetics of male infertility in the era of next-generation sequencing. Arab J. Urol. *16*, 53–64.
3. Ramalingam, M., Kini, S., and Mahmood, T. (2014). Male fertility and infertility. Obstet. Gynaecol. Reprod. Med. *24*, 326–332.
4. Fujihara, Y., Satouh, Y., Inoue, N., Isotani, A., Ikawa, M., and Okabe, M. (2012). SPACA1-deficient male mice are infertile with abnormally shaped sperm heads reminiscent of globozoospermia. Development *139*, 3583–3589.
5. Ben Khelifa, M., Coutton, C., Zouari, R., Karaouzène, T., Rendu, J., Bidart, M., Yassine, S., Pierre, V., Delaroche, J., Hennebicq, S., et al. (2014). Mutations in DNAH1, which encodes an inner arm heavy chain dynein, lead to male infertility from multiple morphological abnormalities of the sperm flagella. Am. J. Hum. Genet. *94*, 95–104.
6. Baccetti, B., Collodel, G., Estenoz, M., Manca, D., Moretti, E., and Piomboni, P. (2005). Gene deletions in an infertile man with sperm fibrous sheath dysplasia. Hum. Reprod. *20*, 2790–2794.
7. Amiri-Yekta, A., Coutton, C., Kherraf, Z.E., Karaouzène, T., Le Tanno, P., Sanati, M.H., Sabbaghian, M., Almadani, N., Sadighi

Gilani, M.A., Hosseini, S.H., et al. (2016). Whole-exome sequencing of familial cases of multiple morphological abnormalities of the sperm flagella (MMAF) reveals new DNAH1 mutations. Hum. Reprod. *31*, 2872–2880.
8. Tang, S., Wang, X., Li, W., Yang, X., Li, Z., Liu, W., Li, C., Zhu, Z., Wang, L., Wang, J., et al. (2017). Biallelic mutations in CFAP43 and CFAP44 cause male infertility with multiple morphological abnormalities of the sperm flagella. Am. J. Hum. Genet. *100*, 854–864.
9. Dong, F.N., Amiri-Yekta, A., Martinez, G., Saut, A., Tek, J., Stouvenel, L., Lorès, P., Karaouzène, T., Thierry-Mieg, N., Satre, V., et al. (2018). Absence of CFAP69 causes male infertility due to multiple morphological abnormalities of the flagella in human and mouse. Am. J. Hum. Genet. *102*, 636–648.
10. Kherraf, Z.E., Amiri-Yekta, A., Dacheux, D., Karaouzène, T., Coutton, C., Christou-Kent, M., Martinez, G., Landrein, N., Le Tanno, P., Fourati Ben Mustapha, S., et al. (2018). A homozygous ancestral SVA-insertion-mediated deletion in WDR66 induces multiple morphological abnormalities of the sperm flagellum and male infertility. Am. J. Hum. Genet. *103*, 400–412.
11. Auguste, Y., Delague, V., Desvignes, J.P., Longepied, G., Gnisci, A., Besnier, P., Levy, N., Beroud, C., Megarbane, A., Metzler-Guillemain, C., and Mitchell, M.J. (2018). Loss of calmodulin- and radial-spoke-associated complex protein CFAP251 leads to immotile spermatozoa lacking mitochondria and infertility in men. Am. J. Hum. Genet. *103*, 413–420.
12. Coutton, C., Martinez, G., Kherraf, Z.E., Amiri-Yekta, A., Boguenet, M., Saut, A., He, X., Zhang, F., Cristou-Kent, M., Escoffier, J., et al. (2019). Bi-allelic mutations in ARMC2 lead to severe astheno-teratozoospermia due to sperm flagellum malformations in humans and mice. Am. J. Hum. Genet. *104*, 331–340.
13. Martinez, G., Kherraf, Z.E., Zouari, R., Fourati Ben Mustapha, S., Saut, A., Pernet-Gallay, K., Bertrand, A., Bidart, M., Hograindleur, J.P., Amiri-Yekta, A., et al. (2018). Whole-exome sequencing identifies mutations in FSIP2 as a recurrent cause of multiple morphological abnormalities of the sperm flagella. Hum. Reprod. *33*, 1973–1984.
14. Liu, W., He, X., Yang, S., Zouari, R., Wang, J., Wu, H., Kherraf, Z.E., Liu, C., Coutton, C., Zhao, R., et al. (2019). Bi-allelic mutations in TTC21A induce asthenoteratospermia in humans and mice. Am. J. Hum. Genet. *104*, 738–748.
15. Lorès, P., Coutton, C., El Khouri, E., Stouvenel, L., Givelet, M., Thomas, L., Rode, B., Schmitt, A., Louis, B., Sakheli, Z., et al. (2018). Homozygous missense mutation L673P in adenylate kinase 7 (AK7) leads to primary male infertility and multiple morphological anomalies of the flagella but not to primary ciliary dyskinesia. Hum. Mol. Genet. *27*, 1196–1211.
16. Coutton, C., Vargas, A.S., Amiri-Yekta, A., Kherraf, Z.E., Ben Mustapha, S.F., Le Tanno, P., Wambergue-Legrand, C., Karaouzène, T., Martinez, G., Crouzy, S., et al. (2018). Mutations in CFAP43 and CFAP44 cause male infertility and flagellum defects in Trypanosoma and human. Nat. Commun. *9*, 686.
17. Shen, Y., Zhang, F., Li, F., Jiang, X., Yang, Y., Li, X., Li, W., Wang, X., Cheng, J., Liu, M., et al. (2019). Loss-of-function mutations in QRICH2 cause male infertility with multiple morphological abnormalities of the sperm flagella. Nat. Commun. *10*, 433.
18. Liu, C., Lv, M., He, X., Zhu, Y., Amiri-Yekta, A., Li, W., Wu, H., Kherraf, Z.E., Liu, W., Zhang, J., et al. (2019). Homozygous mutations in *SPEF2* induce multiple morphological abnormalities of the sperm flagella and male infertility. J. Med. Genet. jmedgenet-2019-106011. https://doi.org/10.1136/jmedgenet-2019-106011.
19. Li, W., Wu, H., Li, F., Tian, S., Kherraf, Z.-E., Zhang, J., Ni, X., Lv, M., Liu, C., Tan, Q., et al. (2019). Biallelic mutations in *CFAP65* cause male infertility with multiple morphological abnormalities of the sperm flagella in humans and mice. J. Med. Genet. jmedgenet-2019-106344. https://doi.org/10.1136/jmedgenet-2019-106344.
20. Kozminski, K.G., Johnson, K.A., Forscher, P., and Rosenbaum, J.L. (1993). A motility in the eukaryotic flagellum unrelated to flagellar beating. Proc. Natl. Acad. Sci. USA *90*, 5519–5523.
21. Ishikawa, H., and Marshall, W.F. (2017). Intraflagellar transport and ciliary dynamics. Cold Spring Harb. Perspect. Biol. *9*, a021998.
22. Zhang, Y., Liu, H., Li, W., Zhang, Z., Zhang, S., Teves, M.E., Stevens, C., Foster, J.A., Campbell, G.E., Windle, J.J., et al. (2018). Intraflagellar transporter protein 140 (IFT140), a component of IFT-A complex, is essential for male fertility and spermiogenesis in mice. Cytoskeleton (Hoboken) *75*, 70–84.
23. Zhang, Y., Liu, H., Li, W., Zhang, Z., Shang, X., Zhang, D., Li, Y., Zhang, S., Liu, J., Hess, R.A., et al. (2017). Intraflagellar transporter protein (IFT27), an IFT25 binding partner, is essential for male fertility and spermiogenesis in mice. Dev. Biol. *432*, 125–139.
24. Shi, L., Zhou, T., Huang, Q., Zhang, S., Li, W., Zhang, L., Hess, R.A., Pazour, G.J., and Zhang, Z. (2019). Intraflagellar transport protein 74 is essential for spermatogenesis and male fertility in micedouble dagger. Biol. Reprod. *101*, 188–199.
25. Knowles, M.R., Zariwala, M., and Leigh, M. (2016). Primary ciliary dyskinesia. Clin. Chest Med. *37*, 449–461.
26. Li, H., and Durbin, R. (2010). Fast and accurate long-read alignment with Burrows-Wheeler transform. Bioinformatics *26*, 589–595.
27. Wang, K., Li, M., and Hakonarson, H. (2010). ANNOVAR: Functional annotation of genetic variants from high-throughput sequencing data. Nucleic Acids Res. *38*, e164.
28. Ashburner, M., Ball, C.A., Blake, J.A., Botstein, D., Butler, H., Cherry, J.M., Davis, A.P., Dolinski, K., Dwight, S.S., Eppig, J.T., et al.; The Gene Ontology Consortium (2000). Gene ontology: Tool for the unification of biology. Nat. Genet. *25*, 25–29.
29. Kanehisa, M., Furumichi, M., Tanabe, M., Sato, Y., and Morishima, K. (2017). KEGG: New perspectives on genomes, pathways, diseases and drugs. Nucleic Acids Res. *45* (D1), D353–D361.
30. Kumar, P., Henikoff, S., and Ng, P.C. (2009). Predicting the effects of coding non-synonymous variants on protein function using the SIFT algorithm. Nat. Protoc. *4*, 1073–1081.
31. Adzhubei, I.A., Schmidt, S., Peshkin, L., Ramensky, V.E., Gerasimova, A., Bork, P., Kondrashov, A.S., and Sunyaev, S.R. (2010). A method and server for predicting damaging missense mutations. Nat. Methods *7*, 248–249.
32. Schwarz, J.M., Cooper, D.N., Schuelke, M., and Seelow, D. (2014). MutationTaster2: Mutation prediction for the deep-sequencing age. Nat. Methods *11*, 361–362.
33. Lek, M., Karczewski, K.J., Minikel, E.V., Samocha, K.E., Banks, E., Fennell, T., O'Donnell-Luria, A.H., Ware, J.S., Hill, A.J., Cummings, B.B., et al.; Exome Aggregation Consortium (2016). Analysis of protein-coding genetic variation in 60,706 humans. Nature *536*, 285–291.

34. McKenna, A., Hanna, M., Banks, E., Sivachenko, A., Cibulskis, K., Kernytsky, A., Garimella, K., Altshuler, D., Gabriel, S., Daly, M., and DePristo, M.A. (2010). The Genome Analysis Toolkit: A MapReduce framework for analyzing next-generation DNA sequencing data. Genome Res. *20*, 1297–1303.
35. Yang, S.M., Li, H.B., Wang, J.X., Shi, Y.C., Cheng, H.B., Wang, W., Li, H., Hou, J.Q., and Wen, D.G. (2015). Morphological characteristics and initial genetic study of multiple morphological anomalies of the flagella in China. Asian J. Androl. *17*, 513–515.
36. Coutton, C., Escoffier, J., Martinez, G., Arnoult, C., and Ray, P.F. (2015). Teratozoospermia: Spotlight on the main genetic actors in the human. Hum. Reprod. Update *21*, 455–485.
37. Cong, L., Ran, F.A., Cox, D., Lin, S., Barretto, R., Habib, N., Hsu, P.D., Wu, X., Jiang, W., Marraffini, L.A., and Zhang, F. (2013). Multiplex genome engineering using CRISPR/Cas systems. Science *339*, 819–823.
38. Wang, H., Yang, H., Shivalila, C.S., Dawlaty, M.M., Cheng, A.W., Zhang, F., and Jaenisch, R. (2013). One-step generation of mice carrying mutations in multiple genes by CRISPR/Cas-mediated genome engineering. Cell *153*, 910–918.
39. Lu, Y., Oura, S., Matsumura, T., Oji, A., Sakurai, N., Fujihara, Y., Shimada, K., Miyata, H., Tobita, T., Noda, T., et al. (2019). CRISPR/Cas9-mediated genome editing reveals 30 testis-enriched genes dispensable for male fertility in mice. Biol. Reprod. *101*, 501–511.
40. Wang, L., Li, M.Y., Qu, C., Miao, W.Y., Yin, Q., Liao, J., Cao, H.T., Huang, M., Wang, K., Zuo, E., et al. (2017). CRISPR-Cas9-mediated genome editing in one blastomere of two-cell embryos reveals a novel Tet3 function in regulating neocortical development. Cell Res. *27*, 815–829.
41. Gu, T.P., Guo, F., Yang, H., Wu, H.P., Xu, G.F., Liu, W., Xie, Z.G., Shi, L., He, X., Jin, S.G., et al. (2011). The role of Tet3 DNA dioxygenase in epigenetic reprogramming by oocytes. Nature *477*, 606–610.
42. Wang, Y., Yang, J., Jia, Y., Xiong, C., Meng, T., Guan, H., Xia, W., Ding, M., and Yuchi, M. (2014). Variability in the morphologic assessment of human sperm: Use of the strict criteria recommended by the World Health Organization in 2010. Fertil. Steril. *101*, 945–949.
43. Chung, M.I., Kwon, T., Tu, F., Brooks, E.R., Gupta, R., Meyer, M., Baker, J.C., Marcotte, E.M., and Wallingford, J.B. (2014). Coordinated genomic control of ciliogenesis and cell movement by RFX2. eLife *3*, e01439.
44. Takei, R., Katoh, Y., and Nakayama, K. (2018). Robust interaction of IFT70 with IFT52-IFT88 in the IFT-B complex is required for ciliogenesis. Biol. Open *7*, bio033241.
45. Dupont, M.A., Humbert, C., Huber, C., Siour, Q., Guerrera, I.C., Jung, V., Christensen, A., Pouliet, A., Garfa-Traoré, M., Nitschké, P., et al. (2019). Human IFT52 mutations uncover a novel role for the protein in microtubule dynamics and centrosome cohesion. Hum. Mol. Genet. *28*. https://doi.org/10.1093/hmg/ddz1091.
46. Zhang, W., Taylor, S.P., Nevarez, L., Lachman, R.S., Nickerson, D.A., Bamshad, M., Krakow, D., Cohn, D.H.; and University of Washington Center for Mendelian Genomics Consortium (2016). IFT52 mutations destabilize anterograde complex assembly, disrupt ciliogenesis and result in short rib polydactyly syndrome. Hum. Mol. Genet. *25*, 4012–4020.
47. Yin, Q., Shen, J., Wan, X., Liu, Q., Zhou, Y., and Zhang, Y. (2018). Impaired sperm maturation in conditional Lcn6 knockout mice. Biol. Reprod. *98*, 28–41.
48. Guan, M., Bogani, D., Marschall, S., Raspa, M., Takeo, T., Nakagata, N., and Fray, M. (2014). In vitro fertilization in mice using the MBCD-GSH protocol. Curr. Protoc. Mouse Biol. *4*, 67–83.
49. Wambergue, C., Zouari, R., Fourati Ben Mustapha, S., Martinez, G., Devillard, F., Hennebicq, S., Satre, V., Brouillet, S., Halouani, L., Marrakchi, O., et al. (2016). Patients with multiple morphological abnormalities of the sperm flagella due to DNAH1 mutations have a good prognosis following intracytoplasmic sperm injection. Hum. Reprod. *31*, 1164–1172.
50. Allan, R.K., and Ratajczak, T. (2011). Versatile TPR domains accommodate different modes of target protein recognition and function. Cell Stress Chaperones *16*, 353–367.
51. Pazour, G.J., Dickert, B.L., Vucica, Y., Seeley, E.S., Rosenbaum, J.L., Witman, G.B., and Cole, D.G. (2000). Chlamydomonas IFT88 and its mouse homologue, polycystic kidney disease gene tg737, are required for assembly of cilia and flagella. J. Cell Biol. *151*, 709–718.
52. Rosenbaum, J. (2002). Intraflagellar transport. Curr. Biol. *12*, R125.
53. Scholey, J.M. (2003). Intraflagellar transport. Annu. Rev. Cell Dev. Biol. *19*, 423–443.
54. Hou, Y., Qin, H., Follit, J.A., Pazour, G.J., Rosenbaum, J.L., and Witman, G.B. (2007). Functional analysis of an individual IFT protein: IFT46 is required for transport of outer dynein arms into flagella. J. Cell Biol. *176*, 653–665.
55. Brazelton, W.J., Amundsen, C.D., Silflow, C.D., and Lefebvre, P.A. (2001). The bld1 mutation identifies the Chlamydomonas osm-6 homolog as a gene required for flagellar assembly. Curr. Biol. *11*, 1591–1594.
56. Haycraft, C.J., Schafer, J.C., Zhang, Q., Taulman, P.D., and Yoder, B.K. (2003). Identification of CHE-13, a novel intraflagellar transport protein required for cilia formation. Exp. Cell Res. *284*, 251–263.
57. Sun, Z., Amsterdam, A., Pazour, G.J., Cole, D.G., Miller, M.S., and Hopkins, N. (2004). A genetic screen in zebrafish identifies cilia genes as a principal cause of cystic kidney. Development *131*, 4085–4093.
58. Follit, J.A., Tuft, R.A., Fogarty, K.E., and Pazour, G.J. (2006). The intraflagellar transport protein IFT20 is associated with the Golgi complex and is required for cilia assembly. Mol. Biol. Cell *17*, 3781–3792.
59. Palermo, G., Joris, H., Devroey, P., and Van Steirteghem, A.C. (1992). Pregnancies after intracytoplasmic injection of single spermatozoon into an oocyte. Lancet *340*, 17–18.
60. Chemes, H.E., and Alvarez Sedo, C. (2012). Tales of the tail and sperm head aches: Changing concepts on the prognostic significance of sperm pathologies affecting the head, neck and tail. Asian J. Androl. *14*, 14–23.
61. Sha, Y.W., Xu, X., Mei, L.B., Li, P., Su, Z.Y., He, X.Q., and Li, L. (2017). A homozygous CEP135 mutation is associated with multiple morphological abnormalities of the sperm flagella (MMAF). Gene *633*, 48–53.
62. Cooper, T.G., Noonan, E., von Eckardstein, S., Auger, J., Baker, H.W., Behre, H.M., Haugen, T.B., Kruger, T., Wang, C., Mbizvo, M.T., and Vogelsong, K.M. (2010). World Health Organization reference values for human semen characteristics. Hum. Reprod. Update *16*, 231–245.
63. Auger, J., Jouannet, P., and Eustache, F. (2016). Another look at human sperm morphology. Hum. Reprod. *31*, 10–23.

The American Journal of Human Genetics, Volume *105*

Supplemental Data

Bi-allelic Mutations in *TTC29* Cause Male Subfertility with Asthenoteratospermia in Humans and Mice

Chunyu Liu, Xiaojin He, Wangjie Liu, Shenmin Yang, Lingbo Wang, Weiyu Li, Huan Wu, Shuyan Tang, Xiaoqing Ni, Jiaxiong Wang, Yang Gao, Shixiong Tian, Lin Zhang, Jiangshan Cong, Zhihua Zhang, Qing Tan, Jingjing Zhang, Hong Li, Yading Zhong, Mingrong Lv, Jinsong Li, Li Jin, Yunxia Cao, and Feng Zhang

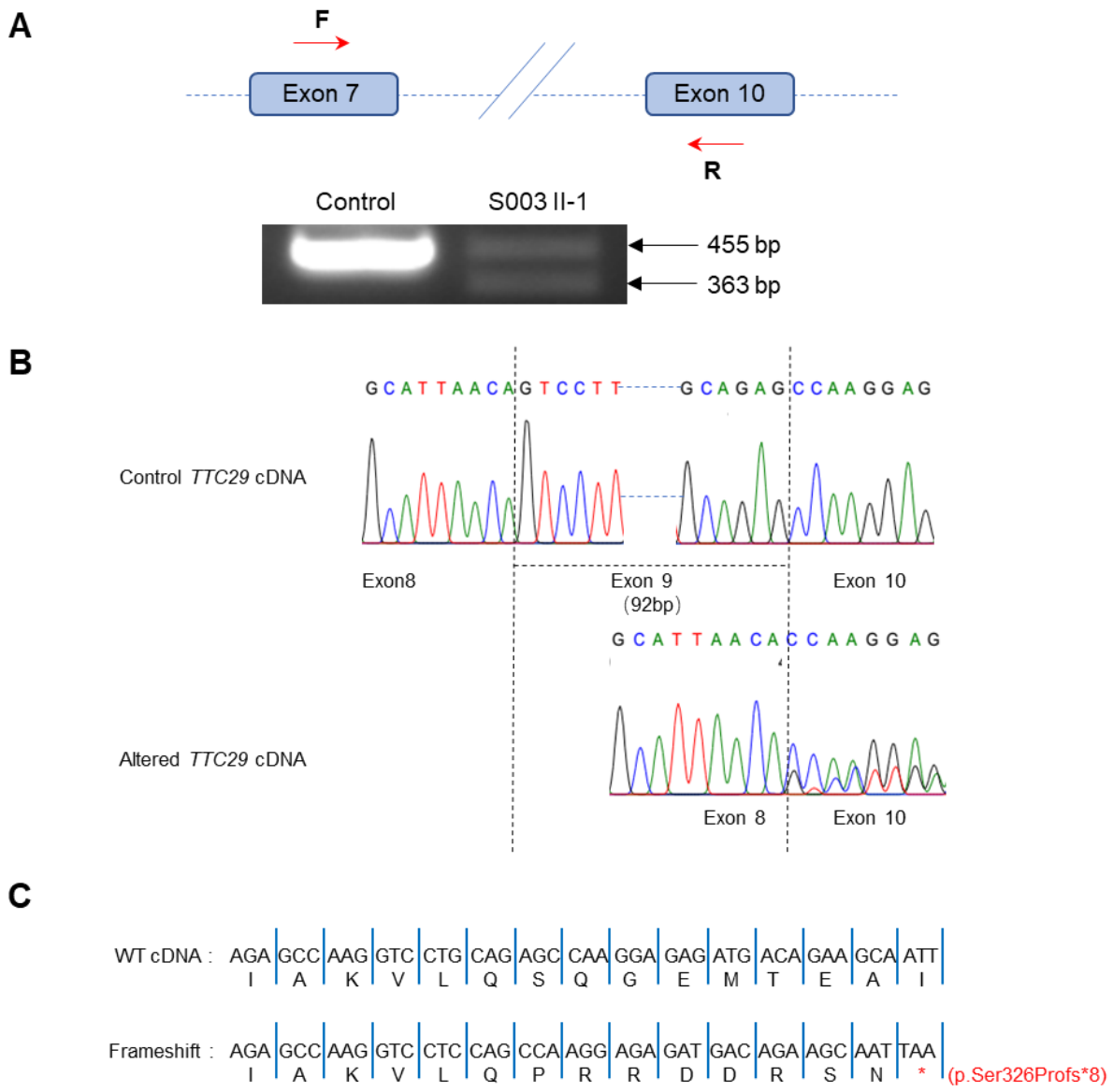

Figure S1. Splicing Alteration Caused by the *TTC29* Splice-Site Mutation in Human Subject S003 II-1.

(A) The forward and reverse primers for cDNA amplification and sequencing were designed in *TTC29* exons 7 and 10, respectively. The RT-PCR product obtained from proband S003 II-1 display two bands; one has same length with a control, but the other is short, suggesting a splicing alteration. (B) Sanger sequencing revealed the skipping of exon 9 in the allele with *TTC29* splice-site mutation c. 977+1G>T in proband S003 II-1. (C) A premature stop codon (p.Ser326Profs*8) was predicted according to the altered cDNA sequence of *TTC29*. Abbreviation: WT, wild-type.

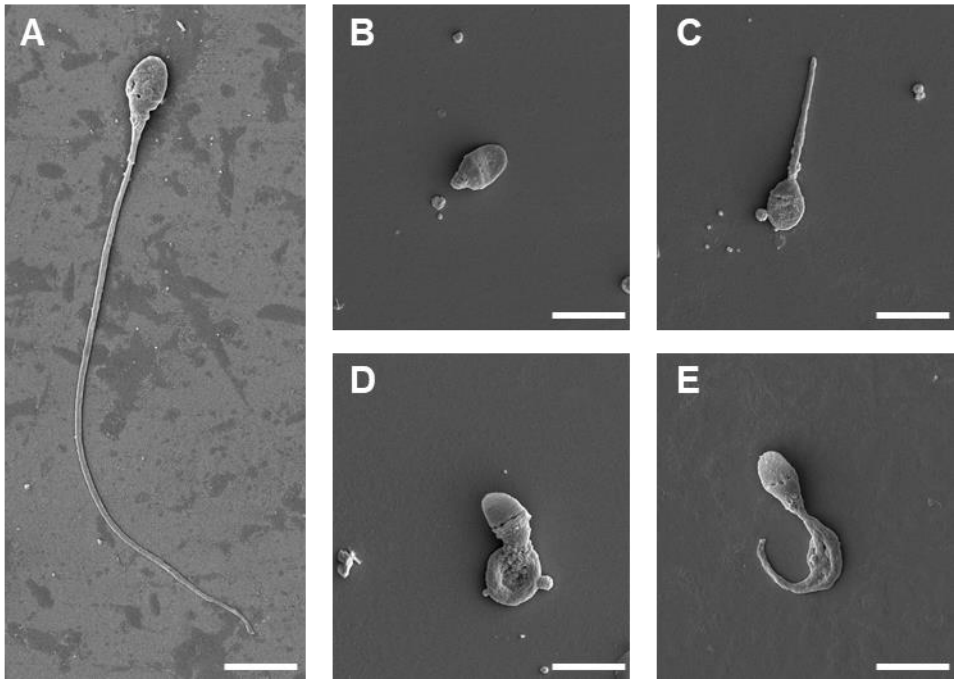

Figure S2. Scanning Electron Microscopy (SEM) Analysis of Spermatozoa from a Normal Male Control and the Men Harboring *TTC29* Mutations.

(A) The SEM image shows normal sperm morphology in the control male. (B-E) SEM images show that most spermatozoa of the men harboring *TTC29* mutations presented with absent, short, coiled or irregular caliber flagella. The data of the *TTC29*-mutated subject A038 IV-1 are exemplified here. Scale bars: 5 μm.

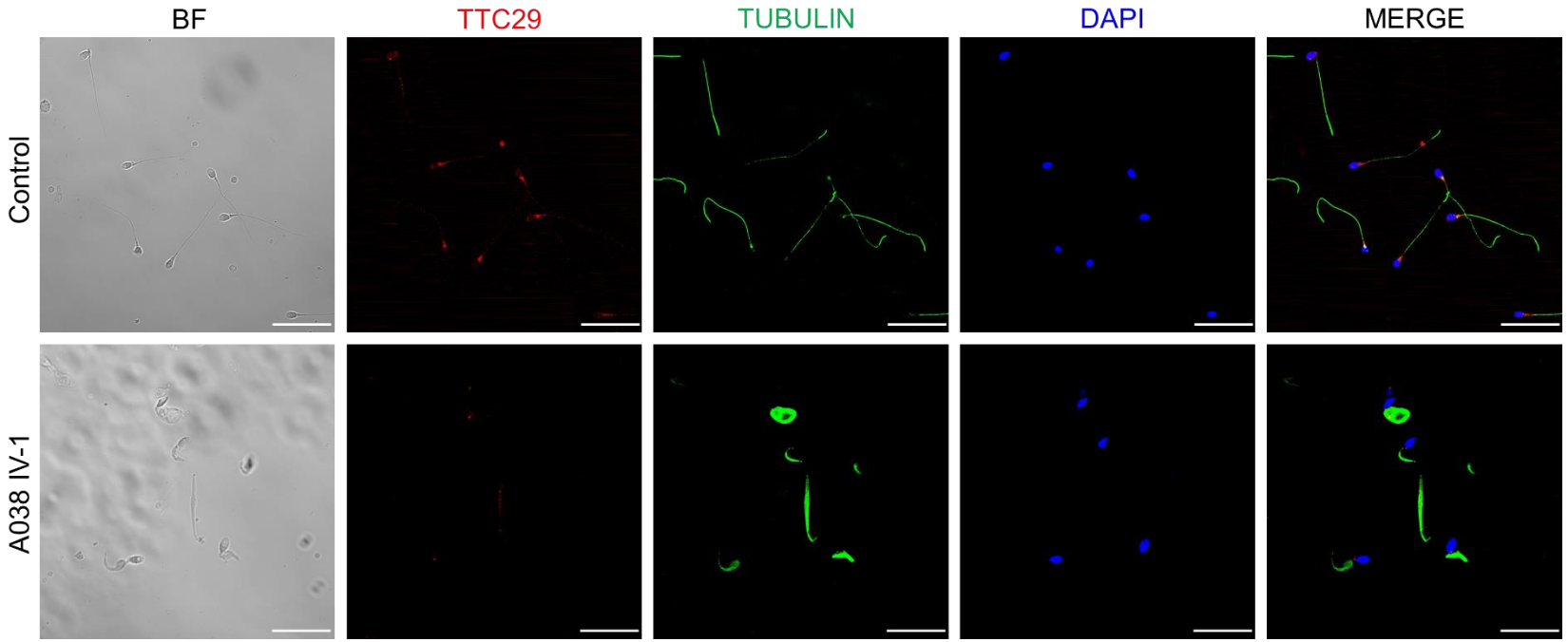

Figure S3. TTC29 Immunostaining in Human Spermatozoa from a Normal Control and a Man Harboring a Homozygous *TTC29* Mutation.

Sperm cells were stained with anti-TTC29 (red) and anti-α-tubulin (green) antibodies. DNA was counterstained with DAPI as a nuclei marker. The images of spermatozoa from subject A038 IV-1 are given as examples of typical staining observed in patients. Scale bars: 20 μm.

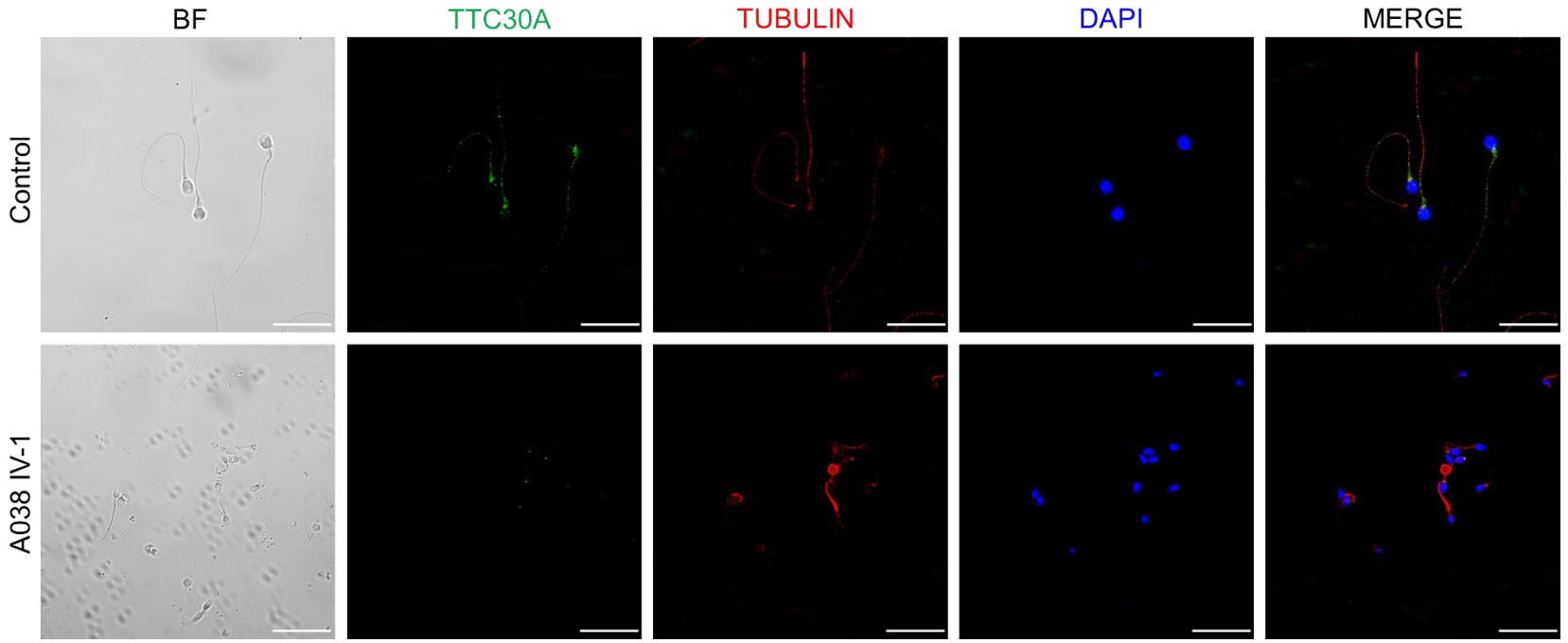

Figure S4. TTC30A Immunostaining in Human Spermatozoa from a Normal Control and a Man Harboring a Homozygous *TTC29* Mutation.

Sperm cells were stained with anti-TTC30A (green) and anti-α-tubulin (red) antibodies. DNA was counterstained with DAPI as a nuclei marker. TTC30A immunostaining can be detected in spermatozoa from a normal control, but is absent in those from the man harboring a homozygous *TTC29* mutation. The images of spermatozoa from subject A038 IV-1 are given as examples of typical staining observed in patients. Scale bars: 20 μm.

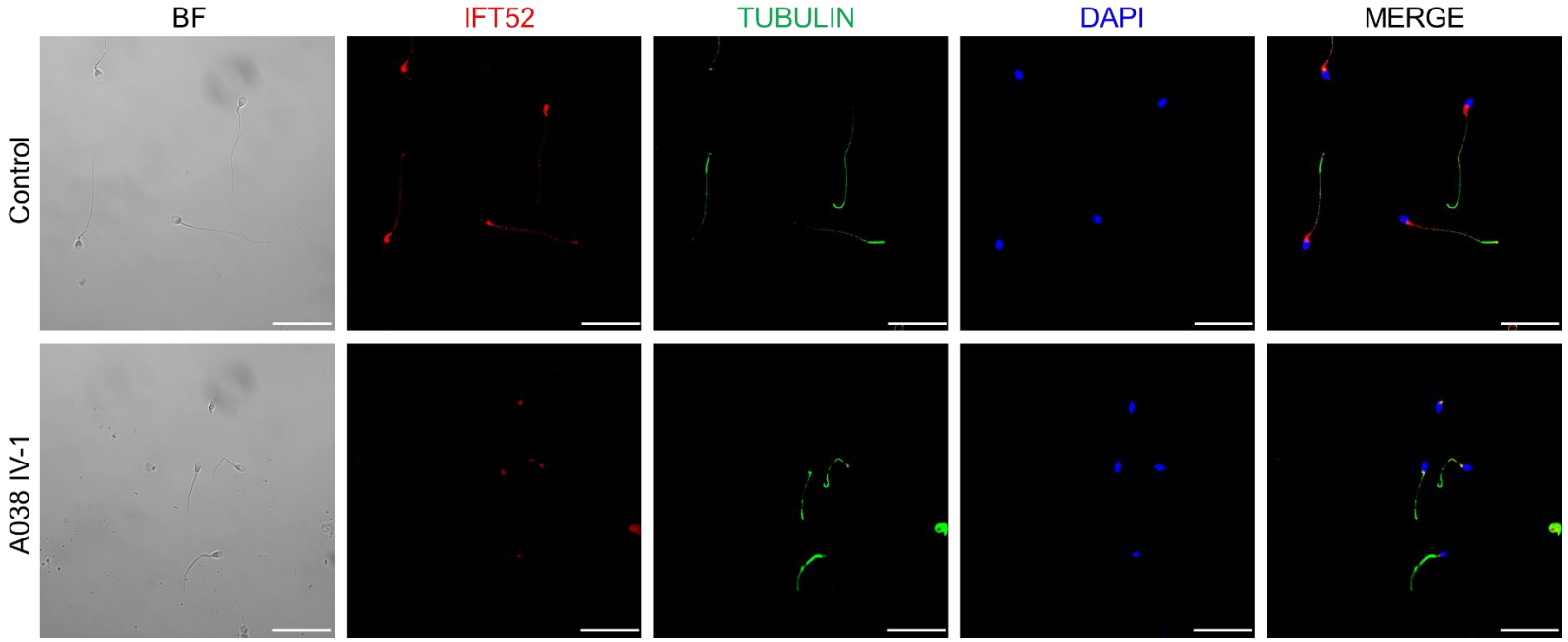

Figure S5. IFT52 Immunostaining in Human Spermatozoa from a Normal Control and a Man Harboring a Homozygous *TTC29* Mutation.

Sperm cells were stained with anti-IFT52 (red) and anti-α-tubulin (green) antibodies. DNA was counterstained with DAPI as a nuclei marker. IFT52 immunostaining revealed a weak staining and only aggregated at the base of sperm flagella in the man harboring a homozygous *TTC29* mutation. The images of spermatozoa from subject A038 IV-1 are given as examples of typical staining observed in patients. Scale bars: 20 µm.

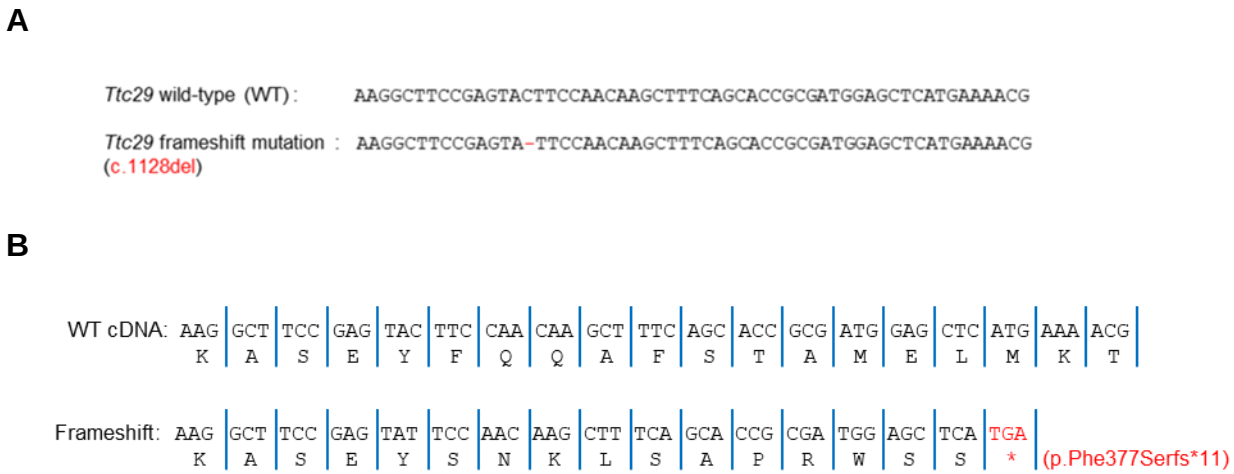

Figure S6. Schematic Illustration of the *Ttc29* Frameshift Mutation Generated in Mice.
(A) A *Ttc29* frameshift mutation (c.1128del) was generated in mice using CRSIPR-Cas9 technology. The deleted nucleotide was shown by a red dash. (B) The frameshift mutation was predicted to cause premature translational termination (p.Phe377Serfs*11) of mouse *Ttc29*. The termination codon (red asterisk) was shown in the mutated cDNA. Abbreviation: WT, wild-type.

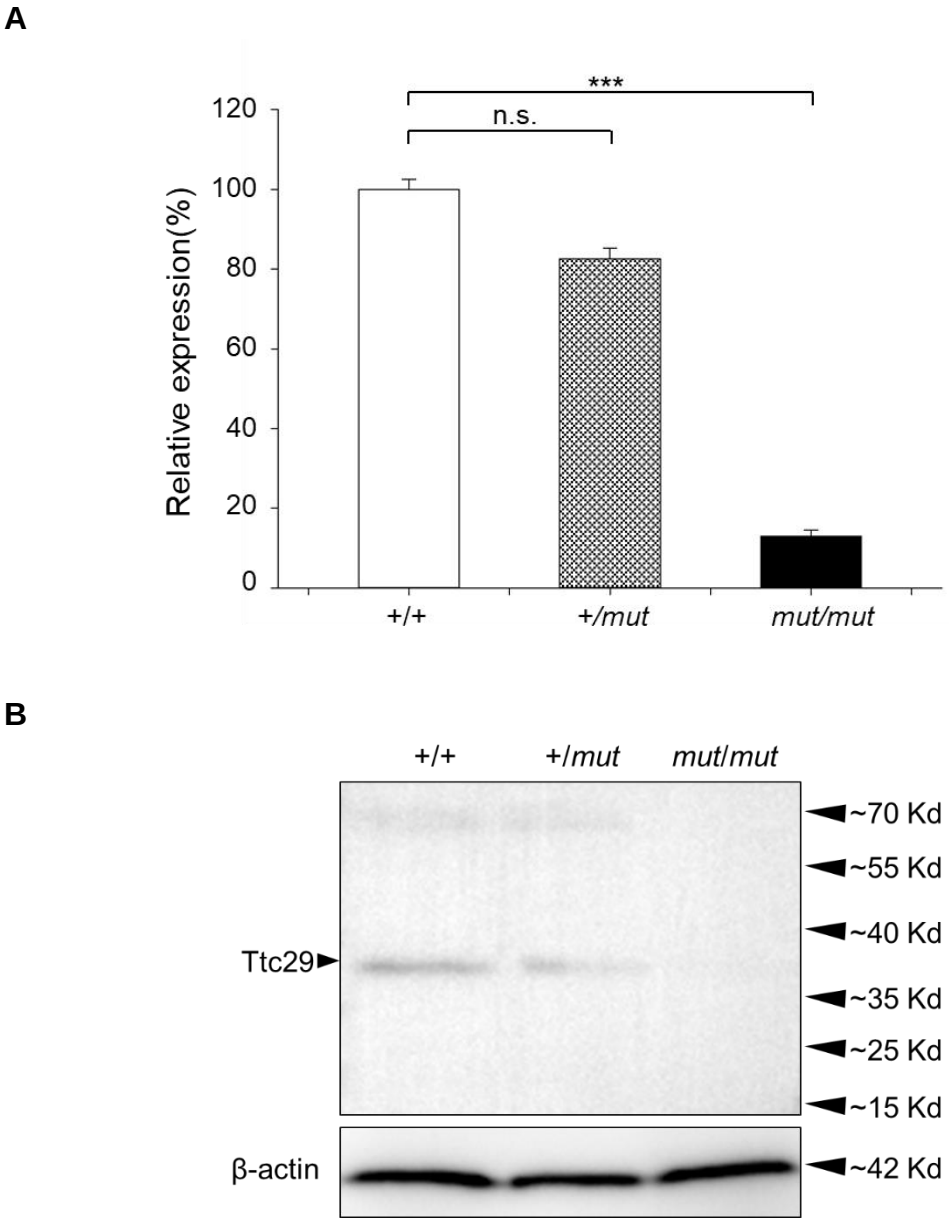

Figure S7. Expression Analysis of *Ttc29*/Ttc29 mRNA and Protein in the *Ttc29*-Mutated Male Mice.

The expression of *Ttc29* mRNA and protein were analyzed in the spermatozoa from wild-type (+/+) male mice, *Ttc29*-mutated (*mut*/*mut*) male mice and heterozygous male carriers (+/*mut*). (A) RT-qPCR assays suggested that the level of *Ttc29* mRNA reduced significantly in the spermatozoa from *Ttc29*-mutated male mice when compared to that of wild-type male mice. Data represent the means ± SEM of three independent experiments. Two-tailed Student's paired or unpaired *t* tests were used as appropriate (*** $P < 0.001$; n.s., not significant). (B) Western blotting analysis revealed the almost absence of Ttc29 protein in the spermatozoa from *Ttc29*-mutated (*mut*/*mut*) male mice. β-actin was used as a loading control.

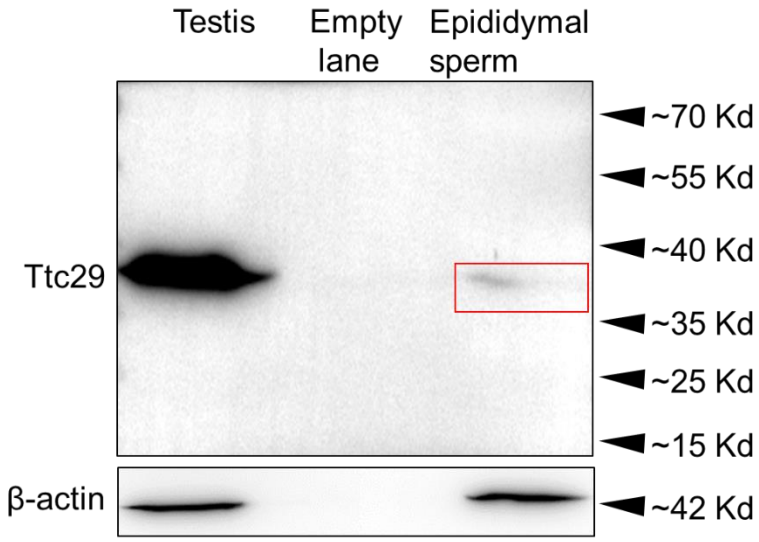

Figure S8. Ttc29 Protein Expressions in Mouse Testis and Epididymal Spermatozoa.
Western blotting analysis revealed the lower expression of Ttc29 protein (indicated by a red box) in the epididymal spermatozoa from wild-type male mice than in mouse testis. An empty lane was added to avoid the cross-contamination between testis and epididymal spermatozoa lanes. β-actin was used as a loading control.

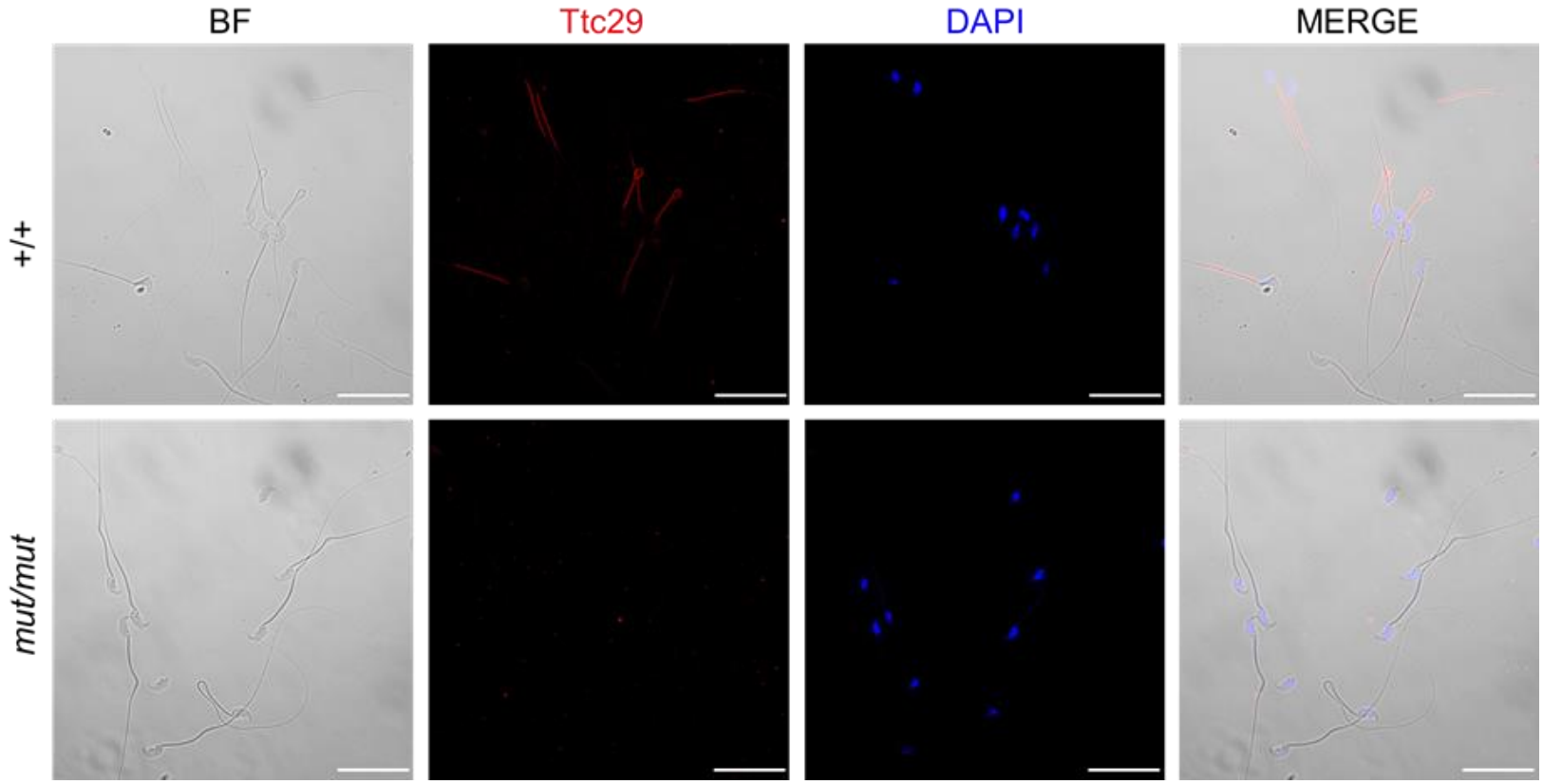

Figure S9. Ttc29 Immunostaining in Spermatozoa from *Ttc29*-Mutated Male Mice.

Mouse sperm cells from wild-type (+/+) and *Ttc29*-mutated (*mut*/*mut*) male mice stained with anti-TTC29 (red) antibody. DNA was counterstained with DAPI. In wild-type male mice, the Ttc29 immunostaining (red) is concentrated in the mid-piece of the sperm flagella and faintly along flagella, but is almost absent in sperm flagella from *Ttc29*-mutated male mice. Scale bars: 20 µm.

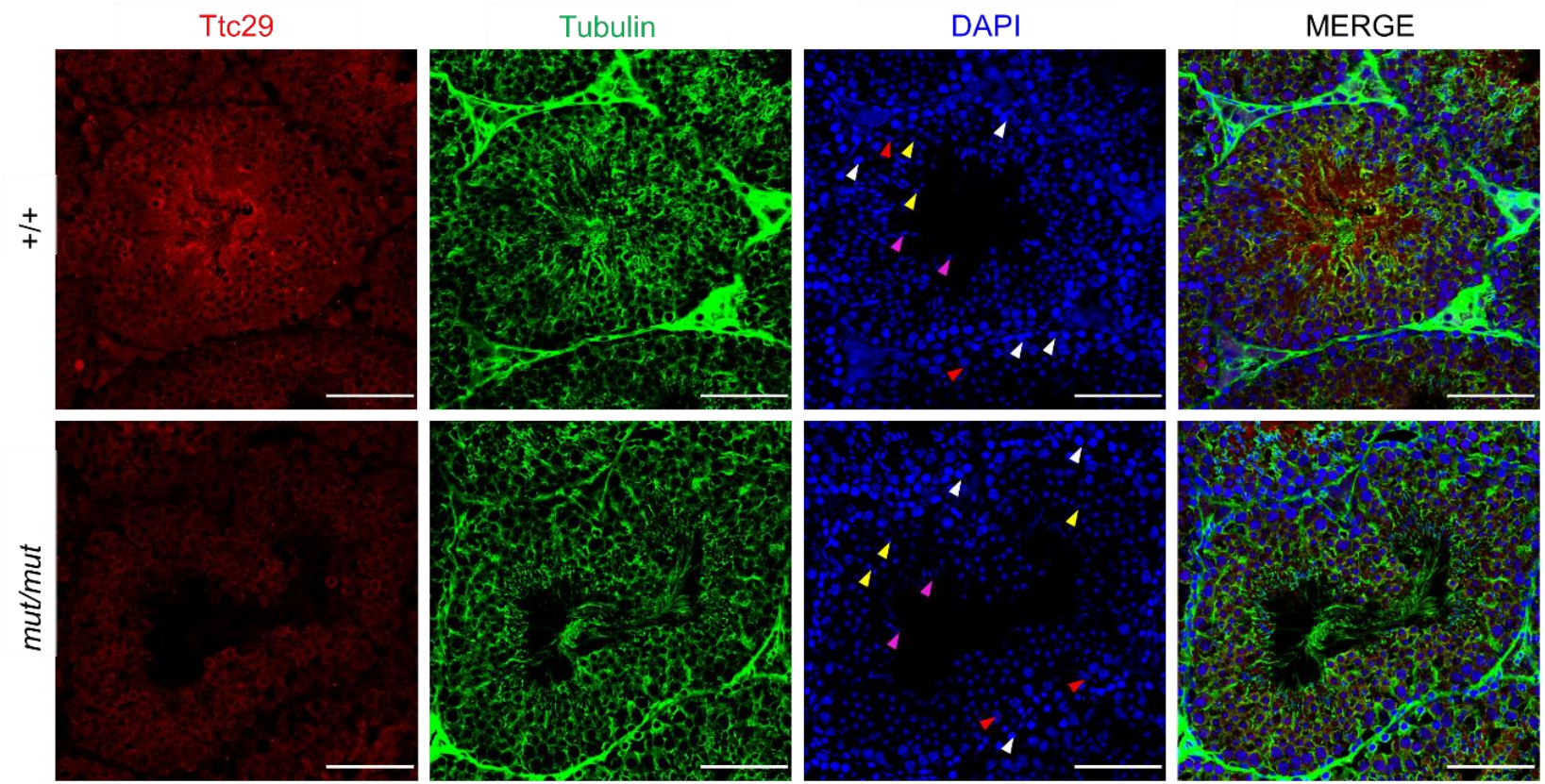

Figure S10. Ttc29 Immunostaining in Cryosections of Testis from *Ttc29*-Mutated Male Mice.
Mouse cryosections of testis from wild-type (+/+) and *Ttc29*-mutated (*mut*/*mut*) male mice stained with anti-TTC29 (red) antibody. DNA was counterstained with DAPI. The Ttc29 immunostaining (red) is mainly concentrated in the elongating spermatids of wild-type male mice, but is significantly reduced in testicular sections from *Ttc29*-mutated male mice. White arrows: zygotene spermatocytes; red arrows: diplotene spermatocytes; yellow arrows: pachytene spermatocytes; pink arrows: elongating spermatids. Scale bars: 100 μm.

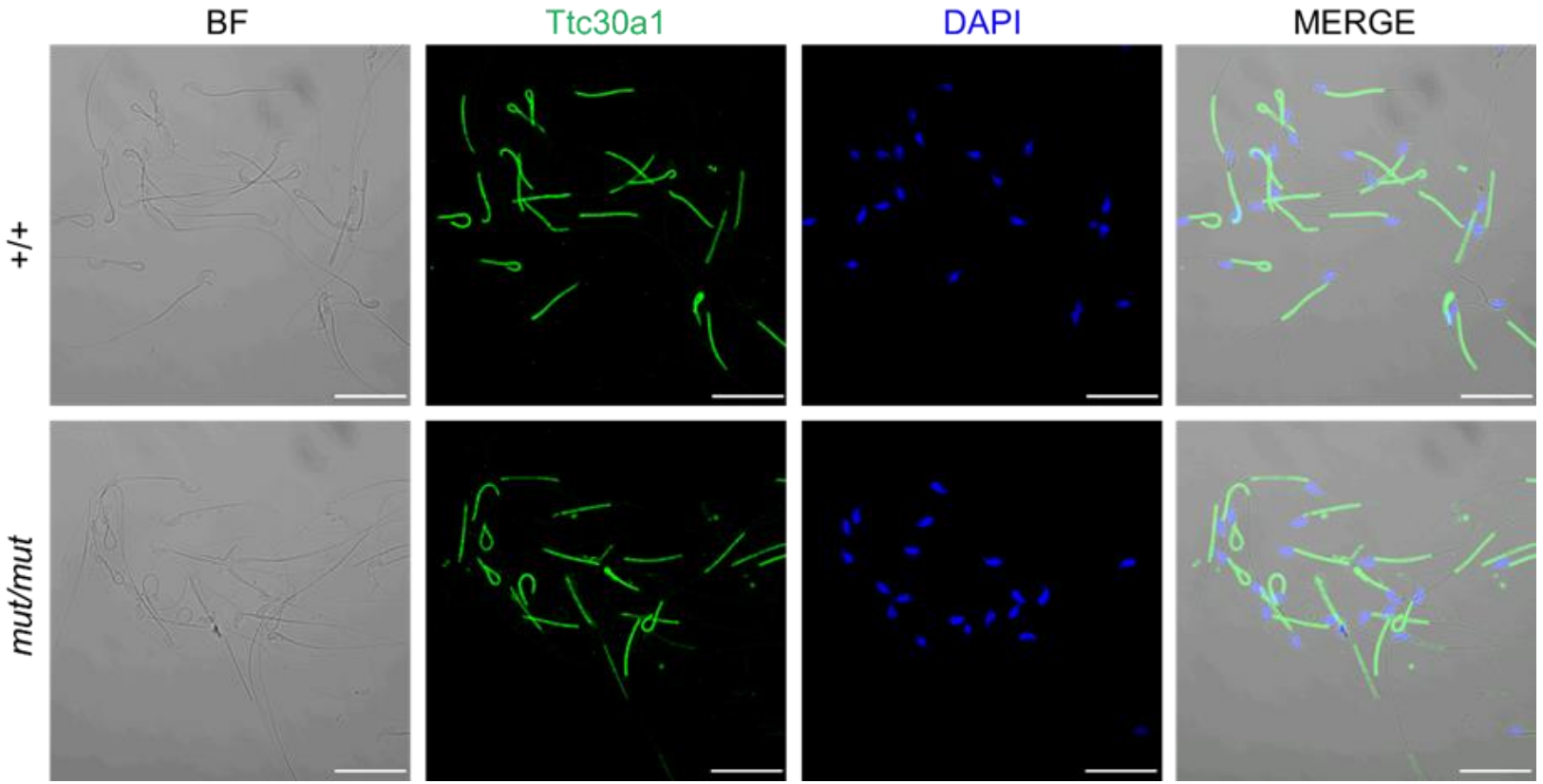

Figure S11. Ttc30a1 Immunostaining in Spermatozoa from *Ttc29*-Mutated Male Mice.
Mouse sperm cells from wild-type (+/+) and *Ttc29*-mutated (*mut*/*mut*) male mice stained with anti-TTC30A (green) antibody. DNA was counterstained with DAPI. The Ttc30a1 immunostaining is found concentrated in the mid-piece of the sperm flagella from both wild-type and *Ttc29*-mutated male mice. Scale bars: 20 μm.

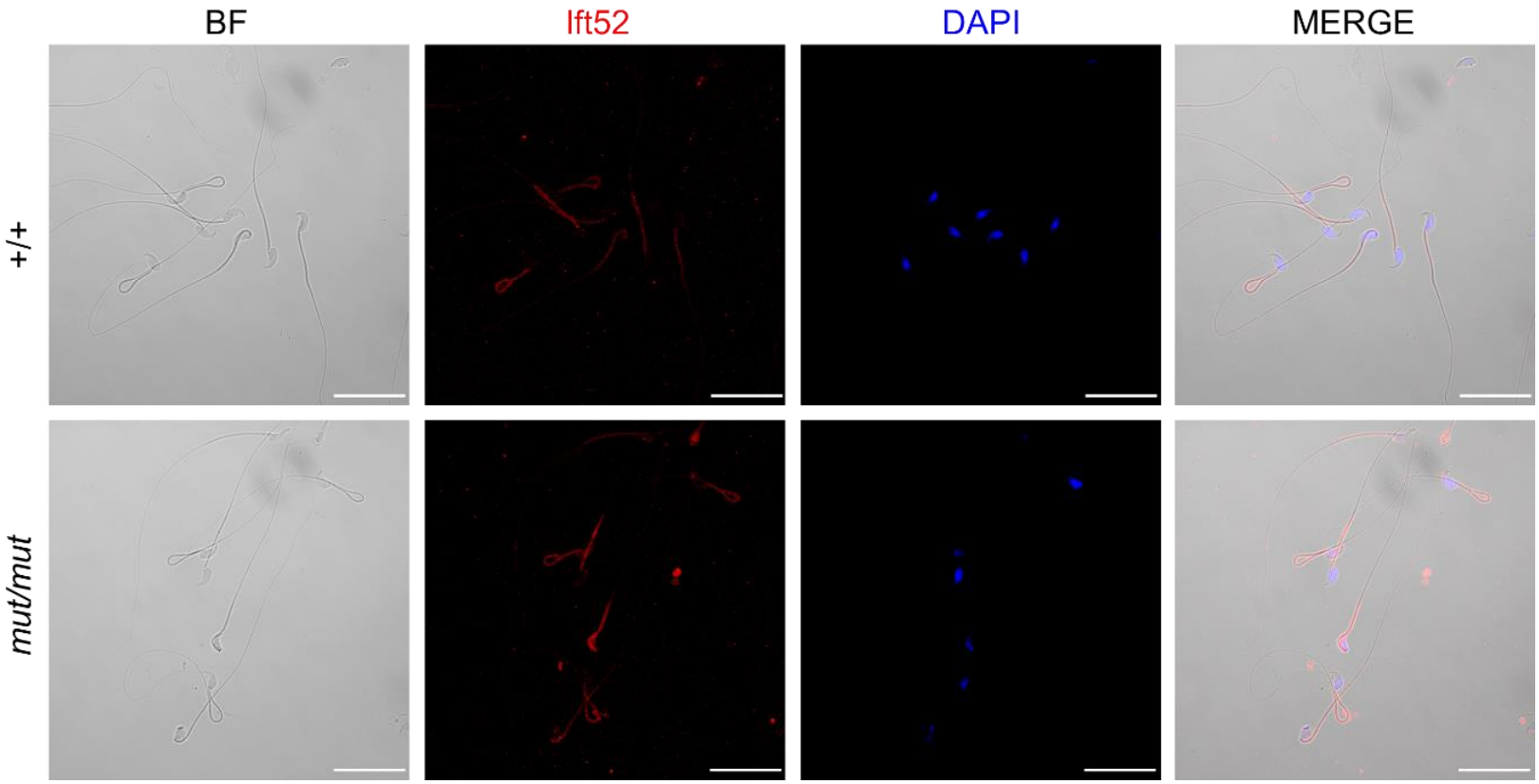

Figure S12. Ift52 Immunostaining in Spermatozoa from *Ttc29*-Mutated Male Mice.
Mouse sperm cells from wild-type (+/+) and *Ttc29*-mutated (*mut*/*mut*) male mice stained with anti-IFT52 (red) antibody. DNA was counterstained with DAPI. The Ift52 immunostaining is detected mainly in the mid-piece of the sperm flagella and faintly along flagella from both wild-type and *Ttc29*-mutated male mice. Scale bars: 20 µm.

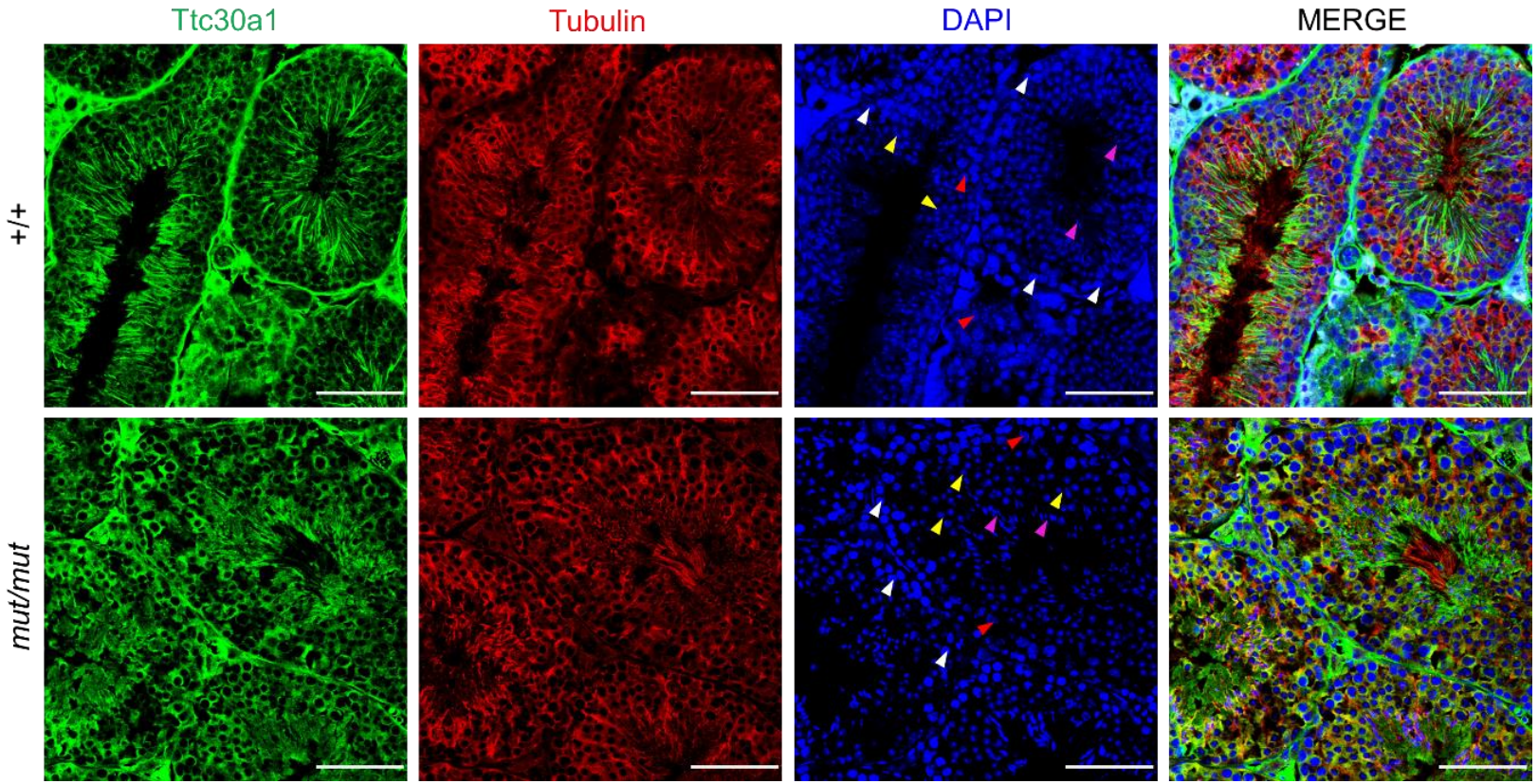

Figure S13. Ttc30a1 Immunostaining in Cryosections of Testis from *Ttc29*-Mutated Male Mice.
Mouse cryosections of testis from wild-type (+/+) and *Ttc29*-mutated (*mut*/*mut*) male mice stained with anti-TTC30A antibody. DNA was counterstained with DAPI. White arrows: zygotene spermatocytes; red arrows: diplotene spermatocytes; yellow arrows: pachytene spermatocytes; pink arrows: elongating spermatids. Scale bars: 100 µm.

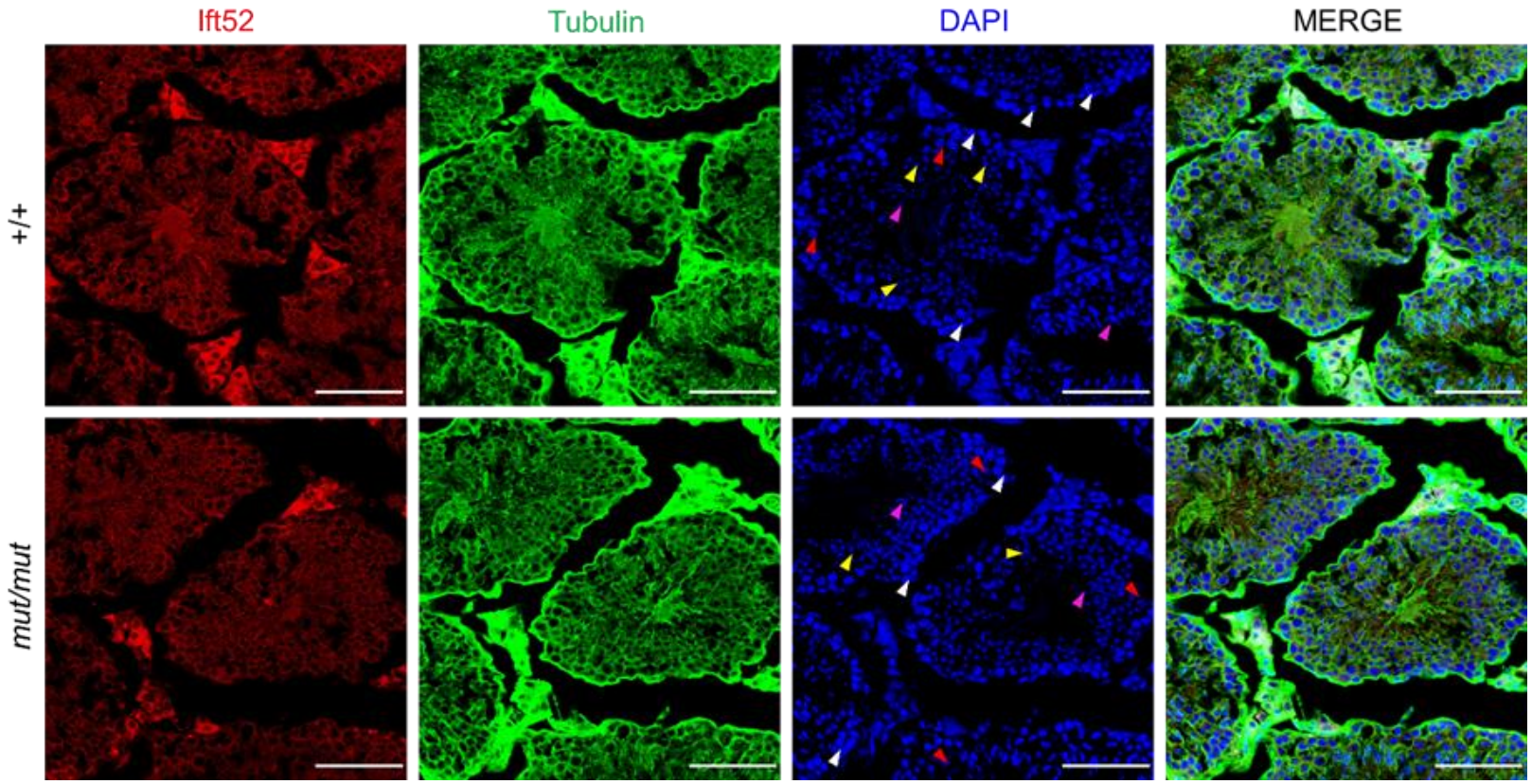

Figure S14. Ift52 Immunostaining in Cryosections of Testis from *Ttc29*-Mutated Male Mice.
Mouse cryosections of testis from wild-type (+/+) and *Ttc29*-mutated (*mut*/*mut*) male mice stained with anti-IFT52 antibody. DNA was counterstained with DAPI. White arrows: zygotene spermatocytes; red arrows: diplotene spermatocytes; yellow arrows: pachytene spermatocytes; pink arrows: elongating spermatids. Scale bars: 100 μm.

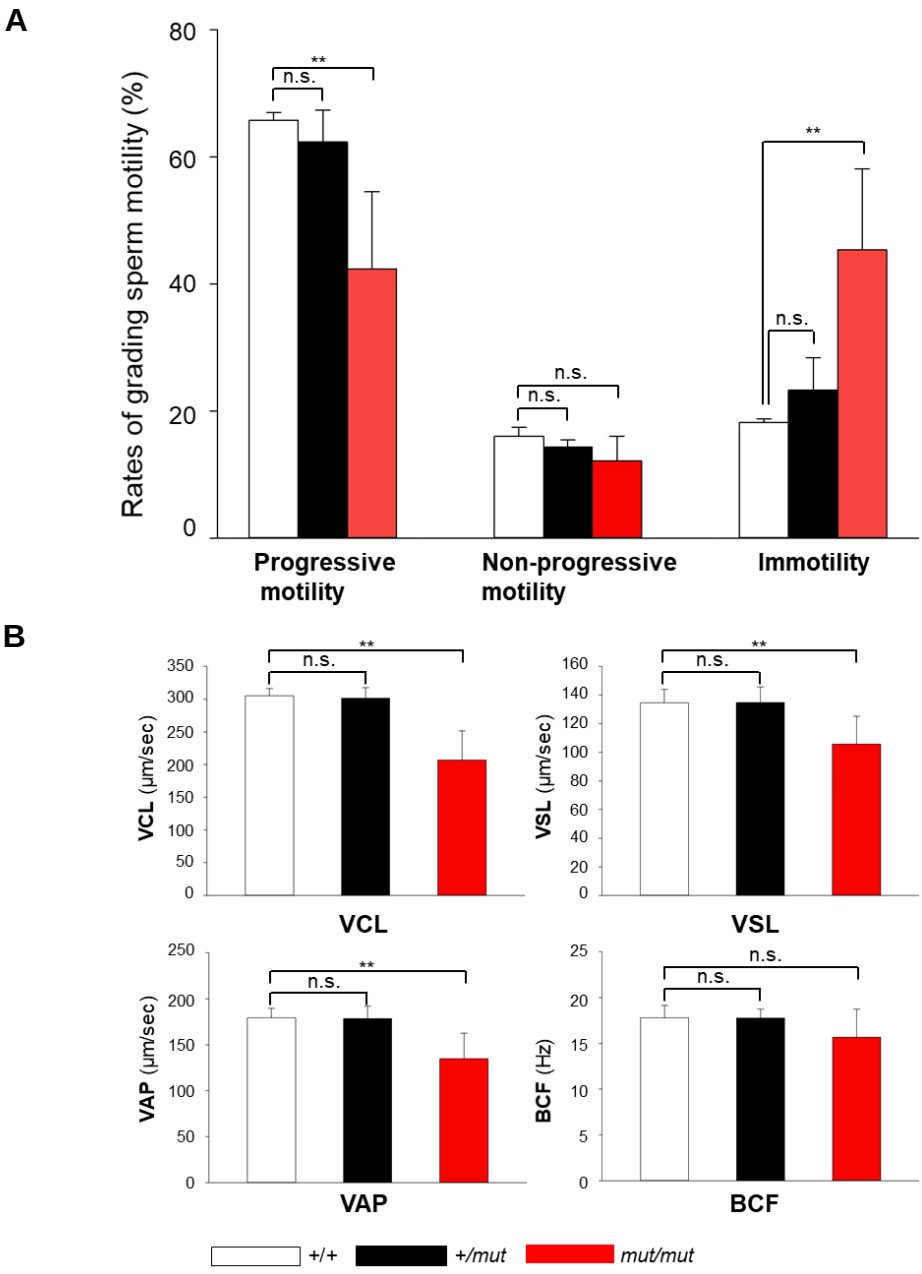

Figure S15. Semen Characteristics of the *Ttc29*-Mutated Male Mice.

(A) The progressive motility, non-progressive motility and immotility are analyzed in spermatozoa of wild-type (+/+), *Ttc29*-mutated (*mut/mut*) male mice and heterozygous male carriers (+/*mut*), respectively. (B) Semen characteristics by computer-assisted analysis system revealed significantly reduced curvilinear velocity (VCL), straight-line velocity (VSL) and average-path velocity (VAP) in *Ttc29*-mutated male mice when compared with those of wild-type male mice. Error bars represent the standard error of the mean. ** $P < 0.01$; n.s., not significant (Student's *t* test). Abbreviation: BCF, beat/cross frequency.

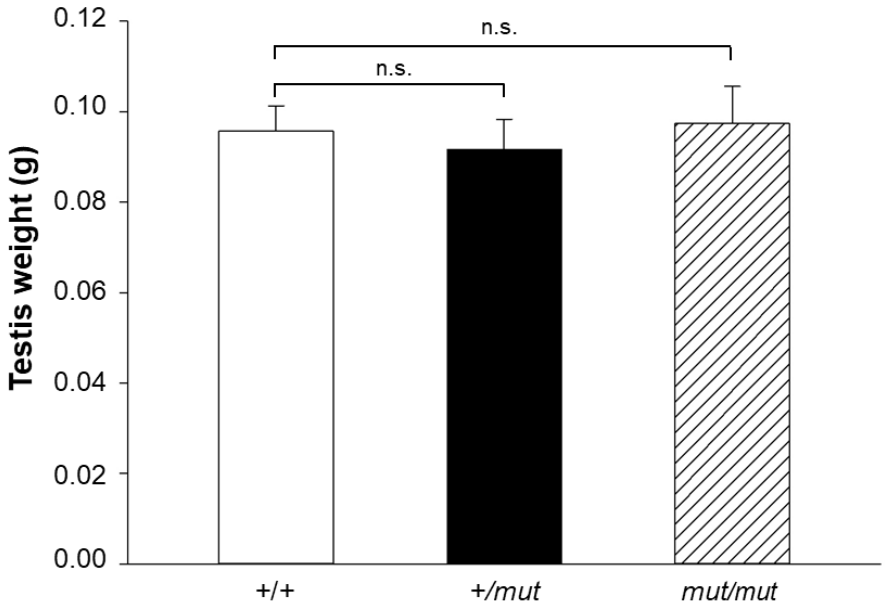

Figure S16. Testis Weights in Wild-Type and *Ttc29*-Mutated Male Mice.
No significant difference was observed in testis weights of *Ttc29*-mutated (*mut/mut*) male mice when compared to wild-type (+/+) male mice. Data represent the means ± SEM; n.s., not significant.

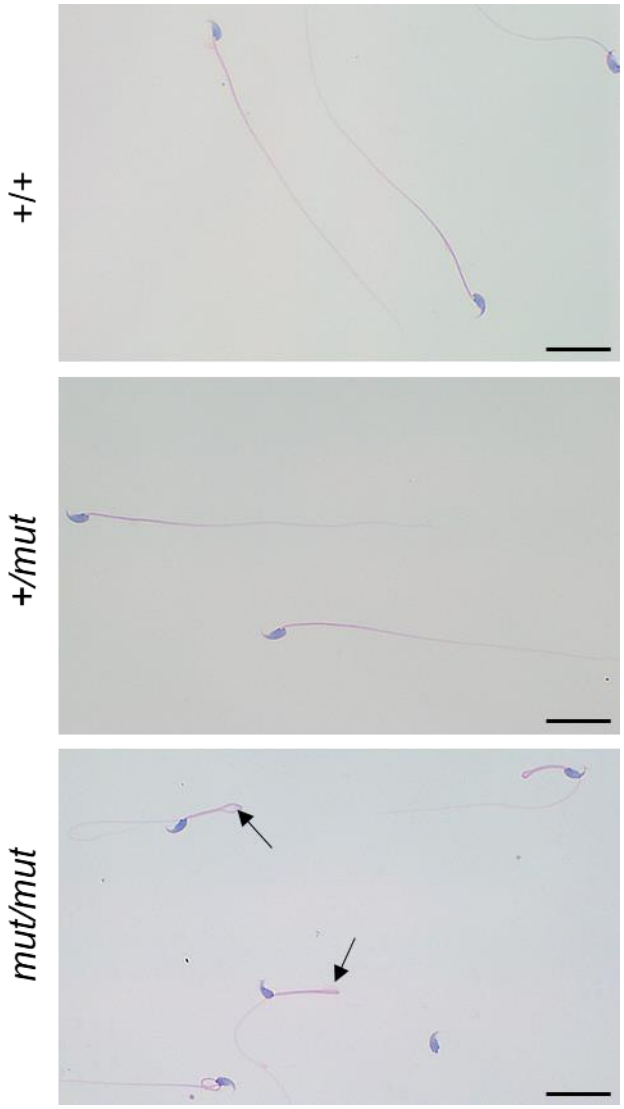

Figure S17. Sperm Morphology of the *Ttc29*-Mutated Male Mice.
Bent flagella was frequently identified in spermatozoa of *Ttc29*-mutated (*mut*/*mut*) male mice when compared with those of wild-type (+/+) male mice and heterozygous male carriers (+/*mut*). Scale bars: 5 μm.

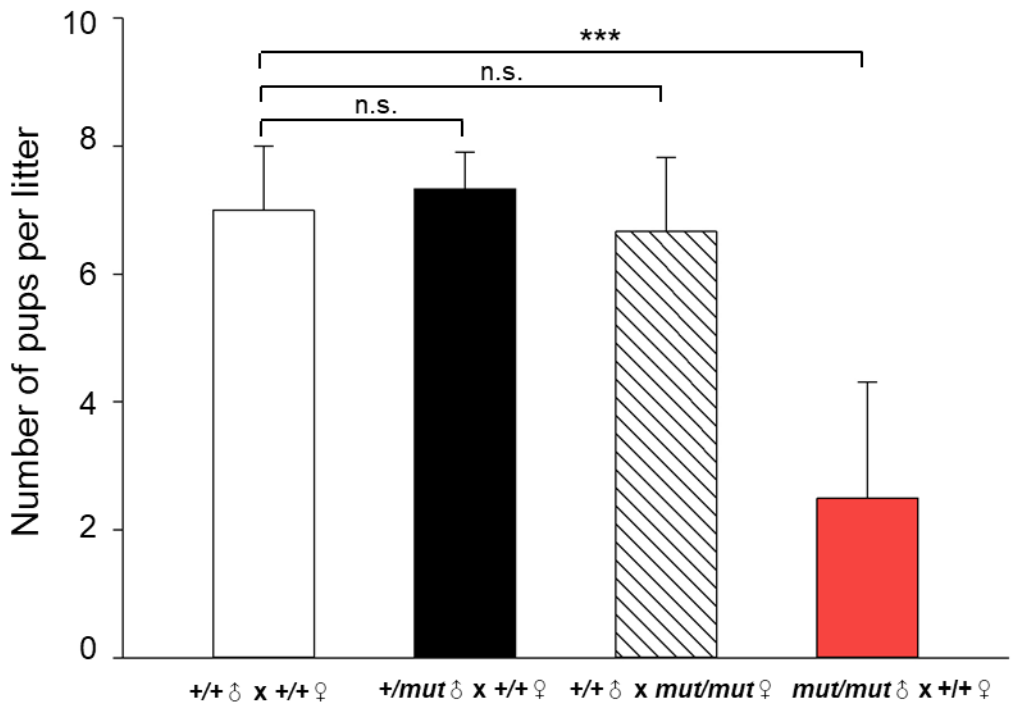

Figure S18. Fertility of Wild-Type and *Ttc29*-Mutated Mice.

Ttc29-mutated (*mut/mut*) male mice and heterozygous male carriers (*+/mut*) were mated with wild-type (+/+) females, and the numbers of pups per litter were counted. No significant difference in fertility was observed between heterozygous male carriers and wild-type male mice. However, the litter sizes of *Ttc29*-mutated males were significantly reduced, and approximately 75% of these males were infertile. *Ttc29*-mutated females were also mated with wild-type males to investigate the effect of *Ttc29* mutations on female mice, but no significant difference was observed between the *Ttc29*-mutated females and wild-type females. Error bars represent the standard error of the mean. *** $P < 0.001$; n.s., not significant (Student's *t* test).

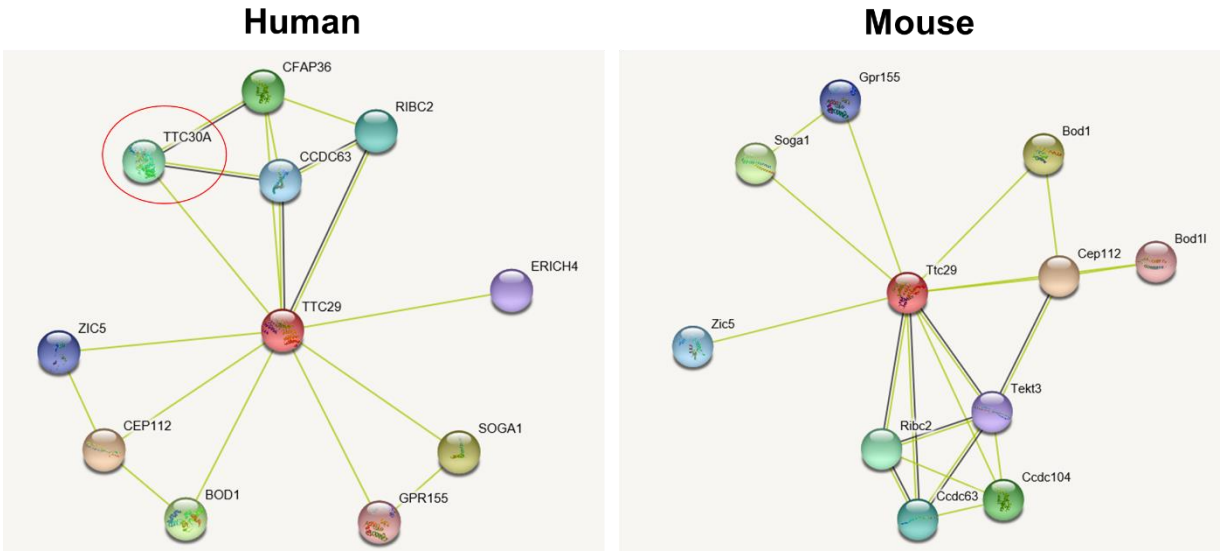

Figure S19. The Protein-Protein Interactions for TTC29/Ttc29 Predicted by STRING.
The protein interaction networks were predicted using *in silico* software String for human and mouse TTC29/Ttc29 proteins, respectively. The direct interaction was predicted between human TTC29 and TTC30A, but no direct interaction was shown between mouse Ttc29 and Ttc30a1. The yellow lines suggest the interactions using text mining, and black lines indicate the identification of co-expression.

Table S1. Bi-allelic Null Mutations of *TTC29* Identified in MMAF-Affected Men

Human subject	*TTC29*		Affected allele	Allele frequency in human population		
	cDNA mutation	Protein alteration		1KGP	ExAC	gnomAD
A002 IV-1	c.1107C>G	p.Tyr369*	Homozygous	0	0	0
A038 IV-1	c. 412_425del	p.Asp138Leufs*10	Homozygous	0	0	0
S003 II-1	c.1107C>G	p.Tyr369*	Heterozygous	0	0	0
	c.977+1G>T	p.Ser326Profs*8	Heterozygous	0	0	0

RefSeq accession number of *TTC29* is NM_031956.3.

Abbreviations: 1KGP, 1000 Genomes Project; ExAC, Exome Aggregation Consortium; gnomAD, Genome Aggregation Database.

Table S2. Primers Used for Amplification and Verification of *TTC29* Mutations

Primer Names	Primer Sequences (5'-3')	Tm
M1-F	AGCATGAGAATGGTGATTTATCAGG	61 ℃
M1-R	CATCTTGCCAGACATTGCAGAACTT	
M2-F	CCTTTCATTCTTTTCATCC	49 ℃
M2-R	TGTTGCTAGTAGGTATTGTCC	
M3-F	TGTGAGATGTGACCCGATTT	56 ℃
M3-R	TTTGGGCAATTATGCAAGAA	
M4-F	GGTAGTTGAGGCTGGTGAGA	53 ℃
M4-R	TTGCCATCTGTTTCTTCTTG	

Table S3. Primers Used for Functional Characteristics of the *TTC29* Splice-Site Mutation

Primer Names	Primer Sequences (5'-3')	Tm
S003-Spl-F	ATTGTAGATGTCCCCAAGCA	54 ℃
S003-Spl-R	GGCGGATATGGAAGGATGAG	

Table S4. Primers Used for Mouse *Ttc29* Genotyping

Primer Names	Primer Sequences (5'-3')	Tm
M-*Ttc29*-F	AGTTCACTTTCCTGCTACCTCCACC	60 ℃
M-*Ttc29*-F	GCCGTTTTACGCTTCTCTTAACCTC	

Table S5. Primers Used for RT-qPCR and RT-PCR Assays

Primer Names	Primer Sequences (5'-3')	Tm
H-*TTC29*-F	TGAATCCGAAATGACCACCC	60 ℃
H-*TTC29*-R	TTCTGGAGGAGCAAGGCAGC	
H-*GAPDH*-F	GGAGCGAGATCCCTCCAAAAT	60 ℃
H-*GAPDH*-R	GGCTGTTGTCATACTTCTCATGG	
M-*Ttc29*-F	CTCGTGAGGACCTACAGATTG	60 ℃
M-*Ttc29*-R	GTTAGTGCGGTTTCATATTCT	
M-*Gapdh*-F	AGGTCGGTGTGAACGGATTTG	60 ℃
M-*Gapdh*-R	TGTAGACCATGTAGTTGAGGTCA	